Exact elasticity solution for natural frequencies of functionally graded simply-supported structures

Exact elasticity solution for natural frequencies of functionally graded simply-supported structures

S. Brischetto*

Abstract

This paper gives an exact three-dimensional elastic model for the free vibration analysis of functionally graded one-layered and sandwich simply-supported plates and shells. An exact elasticity solution is proposed for the differential equations of equilibrium written in general orthogonal curvilinear coordinates. The equations consider a geometry for shells without simplifications, and allow the analysis of the cases of spherical shell panels, cylindrical shell panels, cylindrical closed shells and plates. The main novelty is the possibility of a general formulation for these geometries. The coefficients in equilibrium equations depend on the thickness coordinate because of the radii of curvature for the shell geometries and/or the use of functionally graded layers. These equations are solved in a layer-wise form by introducing a number of mathematical layers where the coefficients are constant. An exhaustive 3D overview of the vibration modes is given for a number of thickness ratios, imposed wave numbers, geometries and embedded materials. Results are given for one-layered functionally graded plates and shells and for sandwich structures with external homogenous skins and an internal core made of functionally graded material. These results can also be used as reference solutions for the validation of analytical or numerical two-dimensional models for functionally graded plates and shells.

Keywords: functionally graded materials, free vibrations, exact solution, three-dimensional analysis, plates, shells.

1 Introduction

Functionally Graded Materials (FGMs) are a new generation of composite materials where two or more constituent phases have a continuously variable composition [Birman and Byrd (2007); Dong and Atluri (2011)]. FGMs present a number of advantages such as a potential reduction of in-plane and transverse through-the-thickness stresses, an improved residual stress distribution, enhanced thermal properties, higher fracture toughness, and reduced stress intensity factors [Bishay et al. (2012); Bishay and Atluri (2012)]. In the design of sandwich structures, the use of FGM cores is a valid alternative to classical cores. Sandwiches with FGM cores have some properties (e.g., the continuity of in-plane stresses in the thickness direction) that sandwiches embedding conventional cores do not have [Brischetto (2009); Carrera and Brischetto (2009)]. The severe temperature loads involved in many engineering applications, such as thermal barrier coatings, engine components or rocket nozzles, require high-temperature resistant materials and high structural performance. The use of FGM structures embedding ceramic

*Corresponding author: Salvatore Brischetto, Assistant Professor, Department of Mechanical and Aerospace Engineering, Politecnico di Torino, Corso Duca degli Abruzzi 24, 10129 Torino, ITALY. tel: +39.011.090.6813, fax: +39.011.090.6899, e.mail: salvatore.brischetto@polito.it.

and metallic phases that continuously vary through the thickness could be an optimal solution for these applications [Brischetto et al. (2008)]. Further FGM applications were described in Mattei et al. (2012) where these materials were used to reproduce biological structures characterized by functional spatially distributed gradients in which each layer has one or more specific functions to perform. FGMs require an accurate evaluation of displacements, strains, stresses and vibrations. These variables are fundamental in the design of FGM structures. Several 2D and 3D models have been developed for the analysis of plate and shell elements embedding functionally graded layers.

Two-dimensional solutions were proposed in the literature for the case of simple problems for one-layered and multilayered FGM structures. Batra and Jin (2005) proposed the first-order shear deformation theory (FSDT) coupled with the finite element method (FEM) to study free vibrations of a functionally graded anisotropic rectangular plate. The first-order shear deformation theory was derived and solved in Efraim and Eisenberger (2007) for various combinations of boundary conditions. The solution was obtained by using the exact element method and the dynamic stiffness method for the free vibrations of annular FGM plates. Annular sectorial FGM plates with simply supported radial edges and arbitrary circular edges were also studied in Nie and Zhong (2008) where the state space method (SSM) and the differential quadrature method (DQM) were used for free and forced vibration analysis. Shariyat (2009) analyzed vibration and dynamic buckling of FGM rectangular plates subjected to thermo-electro-mechanical loading conditions by using a finite element formulation based on a higher-order shear deformation theory. The first-order shear deformation plate theory that uses the element-free *kp*-Ritz method was presented in Zhao et al. (2009) for the free vibration analysis of metal and ceramic functionally graded plates. The use of refined or higher order models for the free vibration analysis of FGM plates was proposed in Dozio (2013) where advanced two-dimensional Ritz-based models are developed. Wu and Chiu (2011) developed the meshless collocation (MC) and element-free Galerkin (EFG) method (using the differential reproducing kernel (DRK) interpolation) for the quasi-three-dimensional free vibration analysis. Further results for free vibration analysis of FGM plates are based on two-dimensional models in closed form solution. Hosseini-Hashemi et al. (2011) used the Reddy third-order shear deformation plate theory. Matsunaga (2008) used a two-dimensional (2-D) higher-order theory. Xia and Shen (2008) developed a higher-order shear deformation plate theory and a general von Karman-type equation for the inclusion of thermal effects. Zenkour (2005b) showed a sinusoidal shear deformation plate theory. Other two-dimensional models for FGM plates consider the static analysis. Zenkour (2005a) investigated deformations in FGM plates via either the shear deformation theories or the classical theories. The extension of Carrera's Unified Formulation to FGM plates was shown in Carrera et al. (2008), Brischetto and Carrera (2010), Brischetto (2009) and Brischetto et al. (2008) where one-layered and sandwich FGM structures were analyzed when subjected to mechanical or thermal loads. Two-dimensional models for the analysis of FGM shells are less numerous than models for FGM plate analysis. Among these, Loy et al. (1999) used strains-displacements relations from Love's shell theory and the eigenvalue governing equation was obtained using Rayleigh-Ritz method. Pradyumna and Bandyopadhyay (2008) analyzed free vibration analysis of functionally graded curved panels by using a higher-order finite element formulation. Matsunaga (2009) extended to shell case the work done in Matsunaga (2008) for two-dimensional (2-D) higher-order plate theory. Wu and Jiang (2012) proposed a quasi-3D model for the analysis of FGM cylinders on the basis of the Reissner Mixed Variational Theorem (RMVT). In another recent model, free vibration analysis of cylindrical shells with holes was investigated by means of a beam model [Cao and Wang (2007)].

An important feature in FGM plate and shell analysis is the use of three-dimensional models. They allow two-dimensional model validations and checks to be made, and they also give further details about three-dimensional effects and their importance. In the literature, three-dimensional solutions for FGM structures are given for specific geometries separately and not in a general framework that is capable to be reduced to different cases such as plates, cylindrical or spherical shells. In a recent study for FGM plates, Dong (2008) investigated three-dimensional free vibrations of functionally graded annular plates

with different boundary conditions using the Chebyshev-Ritz method. Li et al. (2008) analyzed free vibrations of functionally graded material sandwich rectangular plates also using the Chebyshev-Ritz method. A semi-analytical approach composed of differential quadrature method (DQM) and series solution was adopted in Malekzadeh (2009) to solve the equations of motions for the free vibration analysis of thick FGM plates supported on two-parameter elastic foundation. Further three-dimensional models for free vibration analysis of FGM plates used a closed exact solution [Hosseini-Hashemi et al. (2012); Vel and Batra (2004)]. Other three-dimensional exact models allow static analysis of FGM plates. Kashtalyan (2004) and Xu and Zhou (2009) showed the bending of one-layered functionally graded plates. Kashtalyan and Menshykova (2009) investigated the bending of sandwich plates embedding FGM cores. Zhong and Shang (2003) developed an exact three-dimensional analysis for a functionally gradient piezoelectric rectangular plate that was simply supported and grounded along its four edges. Further works analyze FGM shells. Alibeigloo et al. (2012) investigated 3D free vibrations of a functionally graded cylindrical shell embedded in piezoelectric layers. An analytical method for simply supported boundary conditions and a semi-analytical method for non-simply supported conditions were used. Zahedinejad et al. (2010) studied free vibration analysis of functionally graded (FG) curved thick panels under various boundary conditions using the three-dimensional elasticity theory and the differential quadrature method. The trigonometric functions were used to discretize the governing equations. Chen et al. (2004) proposed free vibrations of simply supported, fluid-filled cylindrically orthotropic functionally graded shells with arbitrary thickness. A laminate approximate model was employed that is suitable for an arbitrary variation of material constants along the radial direction. An exact elasticity solution was presented in Vel (2010) for the free and forced vibrations of functionally graded cylindrical shells. Three-dimensional linear elastodynamics equations were used and they were simplified to the case of generalized plane strain deformation in the axial direction. A meshless method based on the local Petrov-Galerkin approach was presented for three-dimensional (3-D) axisymmetric linear elastic solids with continuously varying material properties for the cases of 3D stress analysis of FGM bodies [Sladek et al. (2005)], 3D heat conduction analysis of FGM bodies [Sladek et al. (2008)], and 3D static and elastodynamic analysis of FGM bodies [Sladek et al. (2009)].

In the literature, studies about exact three-dimensional solutions for FGM shells are not so numerous. Moreover, they analyze the various geometries separately and do not give a general framework that is capable to consider different cases such as plates or shells. The present paper aims to fill this gap by proposing a general formulation for the equations of motion in orthogonal curvilinear coordinates that is valid for plates, cylindrical shell panels, spherical shell panels and cylinders embedding layers made of functionally graded material. A general overview is given for those readers interested in both plate and shell analysis. This paper exactly solves the equations of motion in general curvilinear orthogonal coordinates including an exact geometry for shell FGM structures without simplifications. The author used similar approaches for one-layered orthotropic structures and for multilayered orthotropic plates and shells. To the best of the author's knowledge, this is the first time that this solution is proposed by means of the exponential matrix method for the three-dimensional elastic free vibration analysis of FGM plates and shells. The system of second order differential equations is reduced to a system of first order differential equations, and afterwards it is exactly solved by using the exponential matrix method. This methodology has been used in Messina (2009) for the three-dimensional analysis of orthotropic plates in rectilinear orthogonal coordinates, and in Soldatos and Ye (1995) for the exact, three-dimensional, free vibration analysis of angle-ply laminated cylinders in cylindrical coordinates. The equations of motion written in orthogonal curvilinear coordinates allow general exact solutions for plate and shell geometries with constant radii of curvature. The results proposed are for simply supported square plates, cylinders, cylindrical and spherical shell panels made of one FGM layer or for sandwich configurations embedding a functionally graded core. This investigation considers the effects of different functionally graded materials, thickness ratios, geometries, imposed wave numbers, orders of frequencies and vibration modes.

2 Constitutive and geometrical relations

Three-dimensional linear elastic constitutive equations in orthogonal curvilinear coordinates (α, β, z) (see Figure 1) are here given for a generic k isotropic layer [Carrera et al. (2011)]. Coefficients C_{ij} depend on the thickness coordinate z in the case of functionally graded materials. The stress components ($\sigma_{\alpha\alpha}$, $\sigma_{\beta\beta}$, σ_{zz}, $\sigma_{\beta z}$, $\sigma_{\alpha z}$, $\sigma_{\alpha\beta}$) are linked with the strain components ($\epsilon_{\alpha\alpha}$, $\epsilon_{\beta\beta}$, ϵ_{zz}, $\gamma_{\beta z}$, $\gamma_{\alpha z}$, $\gamma_{\alpha\beta}$) for each k FGM layer as:

$$\sigma_{\alpha\alpha k} = C_{11k}(z)\epsilon_{\alpha\alpha k} + C_{12k}(z)\epsilon_{\beta\beta k} + C_{13k}(z)\epsilon_{zzk} \ , \tag{1}$$
$$\sigma_{\beta\beta k} = C_{12k}(z)\epsilon_{\alpha\alpha k} + C_{22k}(z)\epsilon_{\beta\beta k} + C_{23k}(z)\epsilon_{zzk} \ , \tag{2}$$
$$\sigma_{zzk} = C_{13k}(z)\epsilon_{\alpha\alpha k} + C_{23k}(z)\epsilon_{\beta\beta k} + C_{33k}(z)\epsilon_{zzk} \ , \tag{3}$$
$$\sigma_{\beta zk} = C_{44k}(z)\gamma_{\beta zk} \ , \tag{4}$$
$$\sigma_{\alpha zk} = C_{55k}(z)\gamma_{\alpha zk} \ , \tag{5}$$
$$\sigma_{\alpha\beta k} = C_{66k}(z)\gamma_{\alpha\beta k} \ . \tag{6}$$

The strain-displacement relations of three-dimensional theory of elasticity in orthogonal curvilinear coordinates, as also shown in Leissa (1973) and Soedel (2005), are here written for the generic k layer of the multilayered FGM shell with constant radii of curvature (see Figure 1):

$$\epsilon_{\alpha\alpha k} = \frac{1}{H_\alpha}\frac{\partial u_k}{\partial \alpha} + \frac{w_k}{H_\alpha R_\alpha} \ , \tag{7}$$
$$\epsilon_{\beta\beta k} = \frac{1}{H_\beta}\frac{\partial v_k}{\partial \beta} + \frac{w_k}{H_\beta R_\beta} \ , \tag{8}$$
$$\epsilon_{zzk} = \frac{\partial w_k}{\partial z} \ , \tag{9}$$
$$\gamma_{\beta zk} = \frac{1}{H_\beta}\frac{\partial w_k}{\partial \beta} + \frac{\partial v_k}{\partial z} - \frac{v_k}{H_\beta R_\beta} \ , \tag{10}$$
$$\gamma_{\alpha zk} = \frac{1}{H_\alpha}\frac{\partial w_k}{\partial \alpha} + \frac{\partial u_k}{\partial z} - \frac{u_k}{H_\alpha R_\alpha} \ , \tag{11}$$
$$\gamma_{\alpha\beta k} = \frac{1}{H_\alpha}\frac{\partial v_k}{\partial \alpha} + \frac{1}{H_\beta}\frac{\partial u_k}{\partial \beta} \ . \tag{12}$$

The parametric coefficients for shells with constant radii of curvature are:

$$H_\alpha = (1 + \frac{z}{R_\alpha}) = (1 + \frac{\tilde{z} - h/2}{R_\alpha}) \ , \quad H_\beta = (1 + \frac{z}{R_\beta}) = (1 + \frac{\tilde{z} - h/2}{R_\beta}) \ , \quad H_z = 1 \ , \tag{13}$$

h is the total thickness of the structure. H_α and H_β depend on z or $\tilde{z}$ coordinate (see Figure 2). $H_z = 1$ because z coordinate is always rectlinear. R_α and R_β are the principal radii of curvature along the coordinates α and β, respectively. Symbol ∂ indicates the partial derivatives. General geometrical relations for spherical shells in Eqs.(7)-(12) degenerate into geometrical relations for cylindrical shells when R_α or R_β is infinite (with H_α or H_β equals one), and they degenerate into geometrical relations for plates when both R_α and R_β are infinite (with H_α=H_β=1) [Carrera et al. (2011); Leissa (1969)].

Geometrical relations (Eqs.(7)-(12)) are inserted in constitutive equations (Eqs.(1)-(6)) and partial

derivatives $\frac{\partial}{\partial\alpha}$, $\frac{\partial}{\partial\beta}$ and $\frac{\partial}{\partial z}$ are indicated with subscripts $_{,\alpha}$, $_{,\beta}$ and $_{,z}$:

$$\sigma_{\alpha\alpha k} = \frac{C_{11k}(z)}{H_\alpha}u_{k,\alpha} + \frac{C_{11k}(z)}{H_\alpha R_\alpha}w_k + \frac{C_{12k}(z)}{H_\beta}v_{k,\beta} + \frac{C_{12k}(z)}{H_\beta R_\beta}w_k + C_{13k}(z)w_{k,z} \ , \tag{14}$$

$$\sigma_{\beta\beta k} = \frac{C_{12k}(z)}{H_\alpha}u_{k,\alpha} + \frac{C_{12k}(z)}{H_\alpha R_\alpha}w_k + \frac{C_{22k}(z)}{H_\beta}v_{k,\beta} + \frac{C_{22k}(z)}{H_\beta R_\beta}w_k + C_{23k}(z)w_{k,z} \ , \tag{15}$$

$$\sigma_{zzk} = \frac{C_{13k}(z)}{H_\alpha}u_{k,\alpha} + \frac{C_{13k}(z)}{H_\alpha R_\alpha}w_k + \frac{C_{23k}(z)}{H_\beta}v_{k,\beta} + \frac{C_{23k}(z)}{H_\beta R_\beta}w_k + C_{33k}(z)w_{k,z} \ , \tag{16}$$

$$\sigma_{\beta zk} = \frac{C_{44k}(z)}{H_\beta}w_{k,\beta} + C_{44k}(z)v_{k,z} - \frac{C_{44k}(z)}{H_\beta R_\beta}v_k \ , \tag{17}$$

$$\sigma_{\alpha zk} = \frac{C_{55k}(z)}{H_\alpha}w_{k,\alpha} + C_{55k}(z)u_{k,z} - \frac{C_{55k}(z)}{H_\alpha R_\alpha}u_k \ , \tag{18}$$

$$\sigma_{\alpha\beta k} = \frac{C_{66k}(z)}{H_\alpha}v_{k,\alpha} + \frac{C_{66k}(z)}{H_\beta}u_{k,\beta} \ . \tag{19}$$

3 Equilibrium equations

The three differential equations of equilibrium written for the case of free vibration analysis of multilayered spherical shells with constant radii of curvature R_α and R_β are here given (the most general form for variable radii of curvature can be found in Tornabene (2012) and Hildebrand et al. (1949)):

$$H_\beta\frac{\partial\sigma_{\alpha\alpha k}}{\partial\alpha} + H_\alpha\frac{\partial\sigma_{\alpha\beta k}}{\partial\beta} + H_\alpha H_\beta\frac{\partial\sigma_{\alpha zk}}{\partial z} + (\frac{2H_\beta}{R_\alpha} + \frac{H_\alpha}{R_\beta})\sigma_{\alpha zk} = \rho_k(z)H_\alpha H_\beta\ddot{u}_k \ , \tag{20}$$

$$H_\beta\frac{\partial\sigma_{\alpha\beta k}}{\partial\alpha} + H_\alpha\frac{\partial\sigma_{\beta\beta k}}{\partial\beta} + H_\alpha H_\beta\frac{\partial\sigma_{\beta zk}}{\partial z} + (\frac{2H_\alpha}{R_\beta} + \frac{H_\beta}{R_\alpha})\sigma_{\beta zk} = \rho_k(z)H_\alpha H_\beta\ddot{v}_k \ , \tag{21}$$

$$H_\beta\frac{\partial\sigma_{\alpha zk}}{\partial\alpha} + H_\alpha\frac{\partial\sigma_{\beta zk}}{\partial\beta} + H_\alpha H_\beta\frac{\partial\sigma_{zzk}}{\partial z} - \frac{H_\beta}{R_\alpha}\sigma_{\alpha\alpha k} - \frac{H_\alpha}{R_\beta}\sigma_{\beta\beta k} + (\frac{H_\beta}{R_\alpha} + \frac{H_\alpha}{R_\beta})\sigma_{zzk} = \rho_k(z)H_\alpha H_\beta\ddot{w}_k \ , \tag{22}$$

where $\rho_k(z)$ is the mass density that varies through the thickness of a functionally graded layer. $(\sigma_{\alpha\alpha k}, \sigma_{\beta\beta k}, \sigma_{zzk}, \sigma_{\beta zk}, \sigma_{\alpha zk}, \sigma_{\alpha\beta k})$ are the six stress components and $\ddot{u}_k$, $\ddot{v}_k$ and $\ddot{w}_k$ indicate the second temporal derivative of the three displacement components u_k, v_k and w_k, respectively. Each quantity depends on the k layer. R_α and R_β are referred to the mid-surface Ω_0 of the whole multilayered shell. H_α and H_β continuously vary through the thickness of the multilayered shell and they depend on the z thickness coordinate.

The first step is the substitution of the Eqs.(14)-(19) in Eqs.(20)-(22) to obtain a displacement form of the equilibrium relations. This form of differential equations of equilibrium is given for a generic k FGM layer:

$$\Big(-\frac{H_\beta C_{55k}(z)}{H_\alpha R_\alpha^2} - \frac{C_{55k}(z)}{R_\alpha R_\beta}\Big)u_k + \Big(\frac{C_{55k}(z)H_\beta}{R_\alpha} + \frac{C_{55k}(z)H_\alpha}{R_\beta}\Big)u_{k,z} + \Big(\frac{C_{11k}(z)H_\beta}{H_\alpha}\Big)u_{k,\alpha\alpha} + \tag{23}$$
$$\Big(\frac{C_{66k}(z)H_\alpha}{H_\beta}\Big)u_{k,\beta\beta} + \Big(C_{55k}(z)H_\alpha H_\beta\Big)u_{k,zz} + \Big(C_{12k}(z) + C_{66k}(z)\Big)v_{k,\alpha\beta} + \Big(\frac{C_{11k}(z)H_\beta}{H_\alpha R_\alpha} + \frac{C_{12k}(z)}{R_\beta} +$$
$$\frac{C_{55k}(z)H_\beta}{H_\alpha R_\alpha} + \frac{C_{55k}(z)}{R_\beta}\Big)w_{k,\alpha} + \Big(C_{13k}(z)H_\beta + C_{55k}(z)H_\beta\Big)w_{k,\alpha z} = \rho_k(z)H_\alpha H_\beta\ddot{u}_k \ ,$$

$$\Big(-\frac{H_\alpha C_{44k}(z)}{H_\beta R_\beta^2}-\frac{C_{44k}(z)}{R_\alpha R_\beta}\Big)v_k+\Big(\frac{C_{44k}(z)H_\alpha}{R_\beta}+\frac{C_{44k}(z)H_\beta}{R_\alpha}\Big)v_{k,z}+\Big(\frac{C_{66k}(z)H_\beta}{H_\alpha}\Big)v_{k,\alpha\alpha}+ \tag{24}$$
$$\Big(\frac{C_{22k}(z)H_\alpha}{H_\beta}\Big)v_{k,\beta\beta}+\Big(C_{44k}(z)H_\alpha H_\beta\Big)v_{k,zz}+\Big(C_{12k}(z)+C_{66k}(z)\Big)u_{k,\alpha\beta}+\Big(\frac{C_{44k}(z)H_\alpha}{H_\beta R_\beta}+\frac{C_{44k}(z)}{R_\alpha}+$$
$$\frac{C_{22k}(z)H_\alpha}{H_\beta R_\beta}+\frac{C_{12k}(z)}{R_\alpha}\Big)w_{k,\beta}+\Big(C_{44k}(z)H_\alpha+C_{23k}(z)H_\alpha\Big)w_{k,\beta z}=\rho_k(z)H_\alpha H_\beta\ddot{v}_k\ ,$$
$$\Big(\frac{C_{13k}(z)}{R_\alpha R_\beta}+\frac{C_{23k}(z)}{R_\alpha R_\beta}-\frac{C_{11k}(z)H_\beta}{H_\alpha R_\alpha^2}-\frac{2C_{12k}(z)}{R_\alpha R_\beta}-\frac{C_{22k}(z)H_\alpha}{H_\beta R_\beta^2}\Big)w_k+\Big(-\frac{C_{55k}(z)H_\beta}{H_\alpha R_\alpha}+\frac{C_{13k}(z)}{R_\beta}- \tag{25}$$
$$\frac{C_{11k}(z)H_\beta}{H_\alpha R_\alpha}-\frac{C_{12k}(z)}{R_\beta}\Big)u_{k,\alpha}+\Big(-\frac{C_{44k}(z)H_\alpha}{H_\beta R_\beta}+\frac{C_{23k}(z)}{R_\alpha}-\frac{C_{22k}(z)H_\alpha}{H_\beta R_\beta}-\frac{C_{12k}(z)}{R_\alpha}\Big)v_{k,\beta}+$$
$$\Big(\frac{C_{33k}(z)H_\beta}{R_\alpha}+\frac{C_{33k}(z)H_\alpha}{R_\beta}\Big)w_{k,z}+\Big(C_{55k}(z)H_\beta+C_{13k}(z)H_\beta\Big)u_{k,\alpha z}+\Big(C_{44k}(z)H_\alpha+C_{23k}(z)H_\alpha\Big)v_{k,\beta z}+$$
$$\Big(C_{55k}(z)\frac{H_\beta}{H_\alpha}\Big)w_{k,\alpha\alpha}+\Big(C_{44k}(z)\frac{H_\alpha}{H_\beta}\Big)w_{k,\beta\beta}+\Big(C_{33k}(z)H_\alpha H_\beta\Big)w_{k,zz}=\rho_k(z)H_\alpha H_\beta\ddot{w}_k\ .$$

R_α and R_β refer to the reference mid-surface Ω_0 of the multilayered shell. H_α and H_β are calculated through the thickness of the multilayered shell by means of Eq.(13). Equilibrium relations in Eqs.(23)-(25) are for spherical shell panels, they automatically degenerate into equilibrium equations for cylindrical closed/open shell panels when R_α or R_β is infinite (with H_α or H_β equals one) and into equilibrium equations for plates when R_α and R_β are infinite (with H_α and H_β equal one). In this way, a unique and general formulation is possible for any geometry.

Elastic coefficients C_{ij} depend on the thickness coordinate z when the k layer is a functionally graded material layer. Parametric coefficients H_α and H_β depend on the thickness coordinate z in the case of shell geometry and they are equal 1 in case of plates. Therefore, Eqs.(23)-(25) do not have constant coefficients because of FGM layers and/or shell geometry. In order to obtain Eqs.(23)-(25) with constant coefficients, each k layer is divided in l mathematical layers where the coefficients C_{ij} can be assumed as constant and parametric coefficients H_α and H_β can easily be calculated in the middle of each mathematical layer. The Eqs.(23)-(25) can be rewritten by using $j = k \times l$ mathematical layers that allow constant coefficients to be considered [Carrera et al (2008); Brischetto and Carrera (2010)].

The closed form of Eqs.(23)-(25) is obtained for simply supported shells and plates. The three displacement components have the following harmonic form:

$$u_j(\alpha,\beta,z)=U_j(z)e^{i\omega t}cos(\bar{\alpha}\alpha)sin(\bar{\beta}\beta)\ , \tag{26}$$
$$v_j(\alpha,\beta,z)=V_j(z)e^{i\omega t}sin(\bar{\alpha}\alpha)cos(\bar{\beta}\beta)\ , \tag{27}$$
$$w_j(\alpha,\beta,z)=W_j(z)e^{i\omega t}sin(\bar{\alpha}\alpha)sin(\bar{\beta}\beta)\ , \tag{28}$$

where $U_j(z)$, $V_j(z)$ and $W_j(z)$ are the displacement amplitudes in α, β and z directions, respectively. i is the coefficient of the imaginary unit. $\omega = 2\pi f$ is the circular frequency where f is the frequency value, t is the time. In coefficients $\bar{\alpha}=\frac{m\pi}{a}$ and $\bar{\beta}=\frac{n\pi}{b}$, m and n are the half-wave numbers and a and b are the shell dimensions in α and β directions, respectively (calculated in the mid-surface Ω_0).

Eqs.(26)-(28) are substituted in Eqs.(23)-(25) to obtain the following system of equations for each j mathematical layer:

$$\Big(-\frac{C_{55j}H_\beta}{H_\alpha R_\alpha^2}-\frac{C_{55j}}{R_\alpha R_\beta}-\bar{\alpha}^2\frac{C_{11j}H_\beta}{H_\alpha}-\bar{\beta}^2\frac{C_{66j}H_\alpha}{H_\beta}+\rho_j H_\alpha H_\beta\omega^2\Big)U_j+\Big(-\bar{\alpha}\bar{\beta}C_{12j}-\bar{\alpha}\bar{\beta}C_{66j}\Big)V_j+$$
$$\Big(\bar{\alpha}\frac{C_{11j}H_\beta}{H_\alpha R_\alpha}+\bar{\alpha}\frac{C_{12j}}{R_\beta}+\bar{\alpha}\frac{C_{55j}H_\beta}{H_\alpha R_\alpha}+\bar{\alpha}\frac{C_{55j}}{R_\beta}\Big)W_j+\Big(\frac{C_{55j}H_\beta}{R_\alpha}+\frac{C_{55j}H_\alpha}{R_\beta}\Big)U_{j,z}+\Big(\bar{\alpha}C_{13j}H_\beta+ \tag{29}$$

$$
\begin{aligned}
&\bar{\alpha}C_{55j}H_\beta\Big)W_{j,z} + \Big(C_{55j}H_\alpha H_\beta\Big)U_{j,zz} = 0\ ,\\
&\Big(-\bar{\alpha}\bar{\beta}C_{66j} - \bar{\alpha}\bar{\beta}C_{12j}\Big)U_j + \Big(-\frac{C_{44j}H_\alpha}{H_\beta R_\beta^2} - \frac{C_{44j}}{R_\alpha R_\beta} - \bar{\alpha}^2\frac{C_{66j}H_\beta}{H_\alpha} - \bar{\beta}^2\frac{C_{22j}H_\alpha}{H_\beta} + \rho_j H_\alpha H_\beta\omega^2\Big)V_j +\\
&\Big(\bar{\beta}\frac{C_{44j}H_\alpha}{H_\beta R_\beta} + \bar{\beta}\frac{C_{44j}}{R_\alpha} + \bar{\beta}\frac{C_{22j}H_\alpha}{H_\beta R_\beta} + \bar{\beta}\frac{C_{12j}}{R_\alpha}\Big)W_j + \Big(\frac{C_{44j}H_\alpha}{R_\beta} + \frac{C_{44j}H_\beta}{R_\alpha}\Big)V_{j,z} + \Big(\bar{\beta}C_{44j}H_\alpha + \qquad (30)\\
&\bar{\beta}C_{23j}H_\alpha\Big)W_{j,z} + \Big(C_{44j}H_\alpha H_\beta\Big)V_{j,zz} = 0\ ,\\
&\Big(\bar{\alpha}\frac{C_{55j}H_\beta}{H_\alpha R_\alpha} - \bar{\alpha}\frac{C_{13j}}{R_\beta} + \bar{\alpha}\frac{C_{11j}H_\beta}{H_\alpha R_\alpha} + \bar{\alpha}\frac{C_{12j}}{R_\beta}\Big)U_j + \Big(\bar{\beta}\frac{C_{44j}H_\alpha}{H_\beta R_\beta} - \bar{\beta}\frac{C_{23j}}{R_\alpha} + \bar{\beta}\frac{C_{22j}H_\alpha}{H_\beta R_\beta} + \bar{\beta}\frac{C_{12j}}{R_\alpha}\Big)V_j +\\
&\Big(\frac{C_{13j}}{R_\alpha R_\beta} + \frac{C_{23j}}{R_\alpha R_\beta} - \frac{C_{11j}H_\beta}{H_\alpha R_\alpha^2} - \frac{2C_{12j}}{R_\alpha R_\beta} - \frac{C_{22j}H_\alpha}{H_\beta R_\beta^2} - \bar{\alpha}^2\frac{C_{55j}H_\beta}{H_\alpha} - \bar{\beta}^2\frac{C_{44j}H_\alpha}{H_\beta} + \rho_j H_\alpha H_\beta\omega^2\Big)W_j + \qquad (31)\\
&\Big(-\bar{\alpha}C_{55j}H_\beta - \bar{\alpha}C_{13j}H_\beta\Big)U_{j,z} + \Big(-\bar{\beta}C_{44j}H_\alpha - \bar{\beta}C_{23j}H_\alpha\Big)V_{j,z} + \Big(\frac{C_{33j}H_\beta}{R_\alpha} + \frac{C_{33j}H_\alpha}{R_\beta}\Big)W_{j,z} +\\
&\Big(C_{33j}H_\alpha H_\beta\Big)W_{j,zz} = 0\,.
\end{aligned}
$$

Elastic coefficients and mass density can be assumed as constant in each j mathematical layer even if a functionally graded material is considered. Parametric coefficients H_α and H_β are also constant because the thickness coordinate z is known at the middle of each j layer. The system of Eqs.(29)-(31) is written in a compact form by introducing constant coefficients A_{sj} for each block $\Big(\Big)$ with s from 1 to 19:

$$A_{1j}U_j + A_{2j}V_j + A_{3j}W_j + A_{4j}U_{j,z} + A_{5j}W_{j,z} + A_{6j}U_{j,zz} = 0\ , \qquad (32)$$

$$A_{7j}U_j + A_{8j}V_j + A_{9j}W_j + A_{10j}V_{j,z} + A_{11j}W_{j,z} + A_{12j}V_{j,zz} = 0\ , \qquad (33)$$

$$A_{13j}U_j + A_{14j}V_j + A_{15j}W_j + A_{16j}U_{j,z} + A_{17j}V_{j,z} + A_{18j}W_{j,z} + A_{19j}W_{j,zz} = 0\ . \qquad (34)$$

Eqs.(32)-(34) are a system of three second order differential equations. They are written for spherical shell panels with constant radii of curvature but they automatically degenerate into equations for cylindrical shells and plates.

3.1 Solution for multilayered structures

The system of second order differential equations can be reduced to a system of first order differential equations by using the method described in Open Document and Boyce and DiPrima (2001). This methodology is applied to Eqs.(32)-(34):

$$
\begin{bmatrix}
A_{6j} & 0 & 0 & 0 & 0 & 0\\
0 & A_{12j} & 0 & 0 & 0 & 0\\
0 & 0 & A_{19j} & 0 & 0 & 0\\
0 & 0 & 0 & A_{6j} & 0 & 0\\
0 & 0 & 0 & 0 & A_{12j} & 0\\
0 & 0 & 0 & 0 & 0 & A_{19j}
\end{bmatrix}
\begin{bmatrix} U_j\\ V_j\\ W_j\\ U_j'\\ V_j'\\ W_j' \end{bmatrix}'
=
\begin{bmatrix}
0 & 0 & 0 & A_{6j} & 0 & 0\\
0 & 0 & 0 & 0 & A_{12j} & 0\\
0 & 0 & 0 & 0 & 0 & A_{19j}\\
-A_{1j} & -A_{2j} & -A_{3j} & -A_{4j} & 0 & -A_{5j}\\
-A_{7j} & -A_{8j} & -A_{9j} & 0 & -A_{10j} & -A_{11j}\\
-A_{13j} & -A_{14j} & -A_{15j} & -A_{16j} & -A_{17j} & -A_{18j}
\end{bmatrix}
\begin{bmatrix} U_j\\ V_j\\ W_j\\ U_j'\\ V_j'\\ W_j' \end{bmatrix}\ . \qquad (35)
$$

Eq.(35) can be written in a compact form for a generic j layer:

$$\boldsymbol{D}_j\frac{\partial \boldsymbol{U}_j}{\partial \tilde{z}} = \boldsymbol{A}_j\boldsymbol{U}_j\ , \qquad (36)$$

where $\frac{\partial \boldsymbol{U}_j}{\partial \tilde{z}} = \boldsymbol{U}'_j$ and $\boldsymbol{U}_j = [U_j\ V_j\ W_j\ U'_j\ V'_j\ W'_j]$. Eq.(36) can be written as:

$$\boldsymbol{D}_j \boldsymbol{U}'_j = \boldsymbol{A}_j \boldsymbol{U}_j \,, \tag{37}$$

$$\boldsymbol{U}'_j = \boldsymbol{D}_j^{-1} \boldsymbol{A}_j\ \boldsymbol{U}_j \,, \tag{38}$$

$$\boldsymbol{U}'_j = \boldsymbol{A}^*_j\ \boldsymbol{U}_j \,, \tag{39}$$

with $\boldsymbol{A}^*_j = \boldsymbol{D}_j^{-1} \boldsymbol{A}_j$.

In the case of plate geometry coefficients A_{3j}, A_{4j}, A_{9j}, A_{10j}, A_{13j}, A_{14j} and A_{18j} are zero because the radii of curvature R_α and R_β are infinite. The solution of Eq.(39) can be written as [Boyce and DiPrima (2001); Zwillinger (1997)]:

$$\boldsymbol{U}_j(\tilde{z}_j) = exp(\boldsymbol{A}^*_j \tilde{z}_j) \boldsymbol{U}_j(0) \quad \text{with} \quad \tilde{z}_j \,\epsilon\, [0, h_j] \,, \tag{40}$$

where $\tilde{z}_j$ is the thickness coordinate of each j layer from 0 at the bottom to h_j at the top (see Figure 2). The exponential matrix is calculated with $\tilde{z}_j = h_j$ for each j layer as:

$$\boldsymbol{A}^{**}_j = exp(\boldsymbol{A}^*_j h_j) = \boldsymbol{I} + \boldsymbol{A}^*_j\, h_j + \frac{\boldsymbol{A}^{*2}_j}{2!} h_j^2 + \frac{\boldsymbol{A}^{*3}_j}{3!} h_j^3 + \ldots + \frac{\boldsymbol{A}^{*N}_j}{N!} h_j^N \,, \tag{41}$$

where $\boldsymbol{I}$ is the 6×6 identity matrix. This expansion has a fast convergence as indicated in Moler and Van Loan (2003) and it is not time consuming from the computational point of view.

If we consider $j = N_L$ layers, $N_L - 1$ transfer matrices $\boldsymbol{T}_{j-1,j}$ must be calculated by using for each interface the following conditions for interlaminar continuity of displacements and transverse shear/normal stresses:

$$u^b_j = u^t_{j-1}\,,\ \ v^b_j = v^t_{j-1}\,,\ \ w^b_j = w^t_{j-1}\,, \tag{42}$$

$$\sigma^b_{zzj} = \sigma^t_{zzj-1}\,,\ \ \sigma^b_{\alpha zj} = \sigma^t_{\alpha zj-1}\,,\ \ \sigma^b_{\beta zj} = \sigma^t_{\beta zj-1}\,, \tag{43}$$

that means each displacement and transverse stress component at the top (t) of the j-1 layer is equal to displacements and transverse stress components at the bottom (b) of the j layer.
The continuity of transverse shear stress $\sigma_{\alpha z}$ is given as:

$$\frac{C_{55j-1}}{H^t_{\alpha j-1}} \bar{\alpha} W^t_{j-1} + C_{55j-1} U'^t_{j-1} - \frac{C_{55j-1}}{H^t_{\alpha j-1} R_\alpha} U^t_{j-1} = \frac{C_{55j}}{H^b_{\alpha j}} \bar{\alpha} W^b_j + C_{55j} U'^b_j - \frac{C_{55j}}{H^b_{\alpha j} R_\alpha} U^b_j \,, \tag{44}$$

$$U'^b_j = \frac{1}{C_{55j}} \Big(\frac{C_{55j-1}}{H^t_{\alpha j-1}} \bar{\alpha} - \frac{C_{55j}}{H^b_{\alpha j}} \bar{\alpha} \Big) W^t_{j-1} + \frac{1}{C_{55j}} \Big(- \frac{C_{55j-1}}{H^t_{\alpha j-1} R_\alpha} + \frac{C_{55j}}{H^b_{\alpha j} R_\alpha} \Big) U^t_{j-1} + \Big(\frac{C_{55j-1}}{C_{55j}} \Big) U'^t_{j-1} \,. \tag{45}$$

The continuity of transverse shear stress $\sigma_{\beta z}$ is given as:

$$\frac{C_{44j-1}}{H^t_{\beta j-1}} \bar{\beta} W^t_{j-1} + C_{44j-1} V'^t_{j-1} - \frac{C_{44j-1}}{H^t_{\beta j-1} R_\beta} V^t_{j-1} = \frac{C_{44j}}{H^b_{\beta j}} \bar{\beta} W^b_j + C_{44j} V'^b_j - \frac{C_{44j}}{H^b_{\beta j} R_\beta} V^b_j \,, \tag{46}$$

$$V'^b_j = \frac{1}{C_{44j}} \Big(\frac{C_{44j-1}}{H^t_{\beta j-1}} \bar{\beta} - \frac{C_{44j}}{H^b_{\beta j}} \bar{\beta} \Big) W^t_{j-1} + \frac{1}{C_{44j}} \Big(- \frac{C_{44j-1}}{H^t_{\beta j-1} R_\beta} + \frac{C_{44j}}{H^b_{\beta j} R_\beta} \Big) V^t_{j-1} + \Big(\frac{C_{44j-1}}{C_{44j}} \Big) V'^t_{j-1} \,. \tag{47}$$

The continuity of transverse normal stress σ_{zz} is given as:

$$\begin{aligned} &- \frac{C_{13j-1}}{H^t_{\alpha j-1}} \bar{\alpha} U^t_{j-1} + \frac{C_{13j-1}}{H^t_{\alpha j-1} R_\alpha} W^t_{j-1} - \frac{C_{23j-1}}{H^t_{\beta j-1}} \bar{\beta} V^t_{j-1} + \frac{C_{23j-1}}{H^t_{\beta j-1} R_\beta} W^t_{j-1} + C_{33j-1} W'^t_{j-1} = \\ &- \frac{C_{13j}}{H^b_{\alpha j}} \bar{\alpha} U^b_j + \frac{C_{13j}}{H^b_{\alpha j} R_\alpha} W^b_j - \frac{C_{23j}}{H^b_{\beta j}} \bar{\beta} V^b_j + \frac{C_{23j}}{H^b_{\beta j} R_\beta} W^b_j + C_{33j} W'^b_j \,, \end{aligned} \tag{48}$$

$$W_j'^b = \frac{1}{C_{33j}}\Big(- \frac{C_{13j-1}}{H^t_{\alpha j-1}}\bar{\alpha} + \frac{C_{13j}}{H^b_{\alpha j}}\bar{\alpha}\Big)U^t_{j-1} + \frac{1}{C_{33j}}\Big(- \frac{C_{23j-1}}{H^t_{\beta j-1}}\bar{\beta} + \frac{C_{23j}}{H^b_{\beta j}}\bar{\beta}\Big)V^t_{j-1} + \tag{49}$$
$$\frac{1}{C_{33j}}\Big(\frac{C_{13j-1}}{H^t_{\alpha j-1}R_\alpha} + \frac{C_{23j-1}}{H^t_{\beta j-1}R_\beta} - \frac{C_{13j}}{H^b_{\alpha j}R_\alpha} - \frac{C_{23j}}{H^b_{\beta j}R_\beta}\Big)W^t_{j-1} + \Big(\frac{C_{33j-1}}{C_{33j}}\Big)W'^t_{j-1}\,.$$

The continuity of displacement components in Eq.(50) has also been used to obtain the explicit form of Eqs.(45), (47) and (49):

$$U^t_j = U^b_{j-1}\,,\quad V^t_j = V^b_{j-1}\,,\quad W^t_j = W^b_{j-1}\,. \tag{50}$$

In Eqs.(44)-(50), t and b indicate top and bottom of $j-1$ layer and j layer, respectively. $\bar{\alpha}$, $\bar{\beta}$, R_α and R_β refer to mid-surface Ω_0 of the structure. H_α and H_β are calculated at the interfaces between $j-1$ layer and j layer. Eqs.(44)-(50) can be grouped in a system:

$$\begin{bmatrix} U \\ V \\ W \\ U' \\ V' \\ W' \end{bmatrix}^b_j = \begin{bmatrix} 1 & 0 & 0 & 0 & 0 & 0 \\ 0 & 1 & 0 & 0 & 0 & 0 \\ 0 & 0 & 1 & 0 & 0 & 0 \\ T_1 & 0 & T_2 & T_3 & 0 & 0 \\ 0 & T_4 & T_5 & 0 & T_6 & 0 \\ T_7 & T_8 & T_9 & 0 & 0 & T_{10} \end{bmatrix}_{j-1,j} \begin{bmatrix} U \\ V \\ W \\ U' \\ V' \\ W' \end{bmatrix}^t_{j-1}\,, \tag{51}$$

Eq.(51) in compact form is:

$$\boldsymbol{U}^b_j = \boldsymbol{T}_{j-1,j}\boldsymbol{U}^t_{j-1}\,. \tag{52}$$

The calculated $\boldsymbol{T}_{j-1,j}$ matrices allow vector $\boldsymbol{U}$ at the bottom (b) of the j layer with vector $\boldsymbol{U}$ at the top (t) of the $j-1$ layer to be linked. Eq.(52) can also be written as:

$$\boldsymbol{U}_j(0) = \boldsymbol{T}_{j-1,j}\ \boldsymbol{U}_{j-1}(h_{j-1})\,, \tag{53}$$

where $\boldsymbol{U}_j$ is calculated for $\tilde{z}_j = 0$ and $\boldsymbol{U}_{j-1}$ is calculated for $\tilde{z}_{j-1} = h_{j-1}$. $\boldsymbol{U}$ at the top of the j layer is linked with $\boldsymbol{U}$ at the bottom of the same j layer by means of the exponential matrix $\boldsymbol{A}^{**}_j$ in Eq.(41):

$$\boldsymbol{U}_j(h_j) = \boldsymbol{A}^{**}_j\ \boldsymbol{U}_j(0)\,, \tag{54}$$

Eq.(53) can recursively be introduced in Eq.(54) for the $N_L - 1$ interfaces to obtain:

$$\boldsymbol{U}_{N_L}(h_{N_L}) = \boldsymbol{A}^{**}_{N_L}\ \boldsymbol{T}_{N_L-1,N_L}\ \boldsymbol{A}^{**}_{N_L-1}\ \boldsymbol{T}_{N_L-2,N_L-1}\ldots\ldots\boldsymbol{A}^{**}_2\ \boldsymbol{T}_{1,2}\ \boldsymbol{A}^{**}_1\ \boldsymbol{U}_1(0)\,, \tag{55}$$

the definition of the matrix $\boldsymbol{H}_m$ for the multilayered structure allows Eq.(55) to be written as:

$$\boldsymbol{U}_{N_L}(h_{N_L}) = \boldsymbol{H}_m\ \boldsymbol{U}_1(0)\,, \tag{56}$$

that links $\boldsymbol{U}$ calculated at the top of the last N_L layer with $\boldsymbol{U}$ calculated at the bottom of the first layer.

The structures are simply supported and free stresses at the top and at the bottom of the whole multilayered shell, this feature means:

$$\sigma_{zz} = \sigma_{\alpha z} = \sigma_{\beta z} = 0 \quad \text{for} \quad z = -h/2, +h/2 \quad or \quad \tilde{z} = 0, h\,, \tag{57}$$
$$w = v = 0,\ \sigma_{\alpha\alpha} = 0 \quad \text{for} \quad \alpha = 0, a\,, \tag{58}$$
$$w = u = 0,\ \sigma_{\beta\beta} = 0 \quad \text{for} \quad \beta = 0, b\,. \tag{59}$$

Boundary conditions given by Eqs.(58) and (59) are identically satisfied by the displacement field in Eqs. (26)-(28). These boundary conditions do not take part to the determination of the maximal displacement amplitudes addressed in the remaining of the section.

Transverse shear/normal stresses written for a generic value of $\tilde{z}$ in the j layer are:

$$\sigma_{zzj}(\tilde{z}) = -\bar{\alpha}\frac{C_{13j}}{H_\alpha(\tilde{z})}U_j + \frac{C_{13j}}{H_\alpha(\tilde{z})R_\alpha}W_j - \bar{\beta}\frac{C_{23j}}{H_\beta(\tilde{z})}V_j + \frac{C_{23j}}{H_\beta(\tilde{z})R_\beta}W_j + C_{33j}W_{j,z}\,, \tag{60}$$

$$\sigma_{\beta zj}(\tilde{z}) = \bar{\beta}\frac{C_{44j}}{H_\beta(\tilde{z})}W_j + C_{44j}V_{j,z} - \frac{C_{44j}}{H_\beta(\tilde{z})R_\beta}V_j\,, \tag{61}$$

$$\sigma_{\alpha zj}(\tilde{z}) = \bar{\alpha}\frac{C_{55j}}{H_\alpha(\tilde{z})}W_j + C_{55j}U_{j,z} - \frac{C_{55j}}{H_\alpha(\tilde{z})R_\alpha}U_j\,, \tag{62}$$

Imposing Eqs.(57) at the the top (t) of the last N_L layer by using Eqs.(60)-(62) with R_α, R_β, $\bar{\alpha}$ and $\bar{\beta}$ calculated in the mid-surface Ω_0 of the shell, and with H^t_α and H^t_β calculated at top of the whole shell ($\tilde{z} = h$):

$$\sigma^t_{zzN_L} = -\bar{\alpha}\frac{C_{13N_L}}{H^t_\alpha}U^t_{N_L} + \frac{C_{13N_L}}{H^t_\alpha R_\alpha}W^t_{N_L} - \bar{\beta}\frac{C_{23N_L}}{H^t_\beta}V^t_{N_L} + \frac{C_{23N_L}}{H^t_\beta R_\beta}W^t_{N_L} + C_{33N_L}W^t_{N_L,z} = 0\,, \tag{63}$$

$$\sigma^t_{\beta zN_L} = \bar{\beta}\frac{C_{44N_L}}{H^t_\beta}W^t_{N_L} + C_{44N_L}V^t_{N_L,z} - \frac{C_{44N_L}}{H^t_\beta R_\beta}V^t_{N_L} = 0\,, \tag{64}$$

$$\sigma^t_{\alpha zN_L} = \bar{\alpha}\frac{C_{55N_L}}{H^t_\alpha}W^t_{N_L} + C_{55N_L}U^t_{N_L,z} - \frac{C_{55N_L}}{H^t_\alpha R_\alpha}U^t_{N_L} = 0\,, \tag{65}$$

Imposing Eqs.(57) at the the bottom (b) of the first layer ($j = 1$) by using Eqs.(60)-(62) with R_α, R_β, $\bar{\alpha}$ and $\bar{\beta}$ calculated in the mid-surface Ω_0 of the shell, and with H^b_α and H^b_β calculated at bottom of the whole shell ($\tilde{z} = 0$):

$$\sigma^b_{zz1} = -\bar{\alpha}\frac{C_{131}}{H^b_\alpha}U^b_1 + \frac{C_{131}}{H^b_\alpha R_\alpha}W^b_1 - \bar{\beta}\frac{C_{231}}{H^b_\beta}V^b_1 + \frac{C_{231}}{H^b_\beta R_\beta}W^b_1 + C_{331}W^b_{1,z} = 0\,, \tag{66}$$

$$\sigma^b_{\beta z1} = \bar{\beta}\frac{C_{441}}{H^b_\beta}W^b_1 + C_{441}V^b_{1,z} - \frac{C_{441}}{H^b_\beta R_\beta}V^b_1 = 0\,, \tag{67}$$

$$\sigma^b_{\alpha z1} = \bar{\alpha}\frac{C_{551}}{H^b_\alpha}W^b_1 + C_{551}U^b_{1,z} - \frac{C_{551}}{H^b_\alpha R_\alpha}U^b_1 = 0\,. \tag{68}$$

Eqs.(63)-(65) in matrix form are ($\boldsymbol{U}_{N_L}(h_{N_L})$ means $\boldsymbol{U}$ calculated at the top of the whole multilayered shell, last N_L layer with $\tilde{z}_{N_L} = h_{N_L}$):

$$\begin{bmatrix} -\bar{\alpha}\frac{C_{13N_L}}{H^t_\alpha} & -\bar{\beta}\frac{C_{23N_L}}{H^t_\beta} & (\frac{C_{13N_L}}{H^t_\alpha R_\alpha} + \frac{C_{23N_L}}{H^t_\beta R_\beta}) & 0 & 0 & C_{33N_L} \\ 0 & -\frac{C_{44N_L}}{H^t_\beta R_\beta} & \bar{\beta}\frac{C_{44N_L}}{H^t_\beta} & 0 & C_{44N_L} & 0 \\ -\frac{C_{55N_L}}{H^t_\alpha R_\alpha} & 0 & \bar{\alpha}\frac{C_{55N_L}}{H^t_\alpha} & C_{55N_L} & 0 & 0 \end{bmatrix} \begin{bmatrix} U_{N_L}(h_{N_L}) \\ V_{N_L}(h_{N_L}) \\ W_{N_L}(h_{N_L}) \\ U'_{N_L}(h_{N_L}) \\ V'_{N_L}(h_{N_L}) \\ W'_{N_L}(h_{N_L}) \end{bmatrix} = \begin{bmatrix} 0 \\ 0 \\ 0 \end{bmatrix}. \tag{69}$$

Eqs.(66)-(68) in matrix form are ($\boldsymbol{U}_1(0)$ means $\boldsymbol{U}$ calculated at the bottom of the whole multilayered shell, first layer 1 with $\tilde{z}_1 = 0$):

$$\begin{bmatrix} -\bar{\alpha}\frac{C_{131}}{H^b_\alpha} & -\bar{\beta}\frac{C_{231}}{H^b_\beta} & (\frac{C_{131}}{H^b_\alpha R_\alpha} + \frac{C_{231}}{H^b_\beta R_\beta}) & 0 & 0 & C_{331} \\ 0 & -\frac{C_{441}}{H^b_\beta R_\beta} & \bar{\beta}\frac{C_{441}}{H^b_\beta} & 0 & C_{441} & 0 \\ -\frac{C_{551}}{H^b_\alpha R_\alpha} & 0 & \bar{\alpha}\frac{C_{551}}{H^b_\alpha} & C_{551} & 0 & 0 \end{bmatrix} \begin{bmatrix} U_1(0) \\ V_1(0) \\ W_1(0) \\ U'_1(0) \\ V'_1(0) \\ W'_1(0) \end{bmatrix} = \begin{bmatrix} 0 \\ 0 \\ 0 \end{bmatrix}. \tag{70}$$

Eqs.(69) and (70) in compact form to express the free stress state at the top and bottom of the whole shell are:

$$\boldsymbol{B}_{N_L}(h_{N_L})\ \boldsymbol{U}_{N_L}(h_{N_L}) = 0\,, \tag{71}$$

$$\boldsymbol{B}_1(0)\ \boldsymbol{U}_1(0) = 0\,, \tag{72}$$

Eq.(56) can be substituted in Eq.(71) by considering a total number of layers equals N_L:

$$\boldsymbol{B}_{N_L}(h_{N_L})\ \boldsymbol{H}_m\ \boldsymbol{U}_1(0) = 0 \tag{73}$$

Eqs.(72) and (73) are now grouped in the following system:

$$\left[\begin{array}{c} \boldsymbol{B}_{N_L}(h_{N_L})\ \boldsymbol{H}_m \\ \boldsymbol{B}_1(0) \end{array}\right] \left[\ \boldsymbol{U}_1(0)\ \right] = \left[\ \boldsymbol{E}\ \right] \left[\ \boldsymbol{U}_1(0)\ \right] = \left[\ 0\ \right]\,. \tag{74}$$

Matrix $\boldsymbol{E}$ has always (6×6) dimension, independently from the number of layers N_L, even if the method uses a layer-wise approach. The solution is implemented in a Matlab code where only the spherical shell method is considered because it automatically degenerates into cylindrical open/closed shell and plate methods.

The free vibration analysis means to find the non-trivial solution of $\boldsymbol{U}_1(0)$ in Eq.(74) by imposing the determinant of matrix $\boldsymbol{E}$ equals zero:

$$det[\boldsymbol{E}] = 0\,, \tag{75}$$

Eq.(75) means to find the roots of an higher order polynomial in $\lambda = \omega^2$. For each pair of half-wave numbers (m, n) a certain number of circular frequencies are obtained depending on the order N chosen for each exponential matrix $\boldsymbol{A}_j^{**}$ and the number N_L of mathematical layers.

A certain number of circular frequencies ω_s are found when half-wave numbers m and n are imposed in the structures. For each frequency ω_s, it is possible to find the vibration mode through the thickness in terms of the three displacement components. If the frequency ω_s is substituted in the (6×6) matrix $\boldsymbol{E}$, this last matrix has six eigenvalues. We are interested to the null space of matrix $\boldsymbol{E}$ that means to find the (6×1) eigenvector related to the minimum of the six eigenvalues proposed. This null space is the vector $\boldsymbol{U}$ calculated at the bottom of the whole structure for the chosen frequency ω_s:

$$\boldsymbol{U}_{1\omega_s}(0) = \left[\ U_1(0) \quad V_1(0) \quad W_1(0) \quad U_1'(0) \quad V_1'(0) \quad W_1'(0)\ \right]_{\omega_s}^T\,, \tag{76}$$

T means the transpose of the vector and the subscript ω_s means that the null space is calculated for the circular frequency ω_s.

It is possible to find $\boldsymbol{U}_{j\omega_s}(\tilde{z}_j)$ (with the three displacement components $U_{j\omega_s}(\tilde{z}_j)$, $V_{j\omega_s}(\tilde{z}_j)$ and $W_{j\omega_s}(\tilde{z}_j)$ through the thickness) for each j layer of the multilayered structure by using Eqs.(53)-(56) with the index j from 1 to N_L. The thickness coordinate $\tilde{z}$ can assume all the values from the bottom to the top of the structure.

4 Results

The three-dimensional exact solution presented in this paper for the free vibration analysis of functionally graded plates and shells is validated by means of a comparison with two published assessments. The first assessment is the free vibration analysis of a sandwich square plate with an FGM core as proposed in Li et al. (2008). The second assessment is a one-layered FGM cylindrical shell panel as shown in Zahedinejad et al. (2010). After this preliminary validation the method can be used with confidence to investigate the free vibrations of square plates, cylindrical shell panels, cylinders and spherical shell panels (see Figure 3).

4.1 Validation of the method

The first assessment [Li et al. (2008)] considers a simply supported square sandwich plate (see geometry in Figure 3a). The sandwich plate has two external skins with thickness $h_1 = h_3 = 0.1h$ and an internal core with thickness $h_2 = 0.8h$. The bottom skin is ceramic and the top skin is metallic, while the core is made of a functionally graded material. Details about this configuration can be found in Figure 4 and in Li et al. (2008). The metallic (m) material has Young modulus $E_m = 70GPa$, mass density $\rho_m = 2707kg/m^3$ and Poisson ratio $\nu_m = 0.3$. The ceramic (c) material has Young modulus $E_c = 380GPa$, mass density $\rho_c = 3800kg/m^3$ and Poisson ratio $\nu_c = 0.3$. The functionally graded core has constant Poisson ratio $\nu = 0.3$. Young modulus and mass density continuously vary through the thickness direction z as:

$$E(z) = E_m + (E_c - E_m)V_m \,, \tag{77}$$

$$\rho(z) = \rho_m + (\rho_c - \rho_m)V_m \,, \tag{78}$$

where V_m is the volume fraction of the metallic phase that continuously varies through the thickness as:

$$V_m = 1 - V_c = 1 - (0.5 + z/h)^p \,, \tag{79}$$

V_c is the volume fraction of ceramic phase, z varies from $-h/2$ to $h/2$. Exponent p can assume values equal or greater than zero. Li et al. (2008) propose a three-dimensional solution by means of the Ritz approach, and give the fundamental frequency for half-wave numbers $m = n = 1$ and for several thickness ratios a/h and exponents p. The circular frequencies are given in non-dimensional form $\bar{\omega} = \omega \frac{a^2}{h}\sqrt{\frac{\rho_0}{E_0}}$ with $E_0 = 1GPa$ and $\rho_0 = 1kg/m^3$. Table 1 shows the comparison between the model proposed in Li et al. (2008) and the present three-dimensional exact solution. The two methods are in accordance for each thickness ratio a/h and exponent p for the FGM law.

The second assessment [Zahedinejad et al. (2010)] considers a simply supported cylindrical shell panel (see geometry in Figure 3b). The shell has the two dimensions a and b that are coincident ($a = b$), the thickness ratio investigated is a/h equals 5. Two different radii of curvature R_α are considered, that means a/R_α equals 0.5 or 1. The radius of curvature R_β is infinite. The shell is one-layered and is made of a functionally graded material as shown in Figure 4. In this case the structure is fully metallic at the bottom and fully ceramic at the top. This feature means that Eqs.(79) and (80) are still valid, but the volume fraction of ceramic phase V_c is considered in place of the volume fraction of metallic phase V_m:

$$V_c = (0.5 + z/h)^p \,. \tag{80}$$

The metallic phase and the ceramic phase have the properties already seen for the first assessment [Li et al. (2008)]. The only difference is for ρ_m, which is equal to $2702kg/m^3$ (the first assessment considers $\rho_m = 2707kg/m^3$). These material data can be found in Zahedinejad et al. (2010), who propose a three-dimensional differential quadrature method for the free vibration analysis of the cylindrical panel for imposed half-wave numbers $m = n = 1$ and for several exponent values p. The results are given as non-dimensional circular frequencies $\bar{\omega} = \omega h\sqrt{\frac{\rho_c}{E_c}}$. Table 2 shows that the present three-dimensional exact model gives results similar to those obtained with the method proposed by Zahedinejad et al. (2010). The minor differences are due to the fact that the present 3D model is given in exact form while the 3D model in Zahedinejad et al. (2010) is proposed by means of a numerical method such as the differential quadrature method.

In the two proposed assessments, the present 3D solution uses $N_L = 100$ mathematical layers. The exponential matrix in Eq.(41) is approximated with order $N = 3$. The convergence of the approximation is very fast, a small N value is used because of the large number of layers N_L employed to correctly include the curvature effect and the gradation law of the material. The computational cost is low

because the E matrix in Eq.(74) has always 6×6 dimension even if a layer wise approach is employed and $N_L = 100$ mathematical layers are used. The same values of N and N_L are also employed for benchmarks proposed in Section 4.2.

After these two preliminary assessments, the present three-dimensional exact solution can be considered as validated for the free vibration analysis of one-layered and multilayered FGM plates and shells.

4.2 Benchmarks

Four different geometries are considered in the new benchmarks proposed (see Figure 3 for further details). The square plate has dimensions $a = b = 5, 20, 100$ and thickness ratios $a/h = 5, 20, 100$. The cylindrical shell panel has a radius of curvature $R_\alpha = 10$ and an infinite radius of curvature R_β in β direction. The dimensions are $a = \frac{\pi}{3} R_\alpha$ and $b = 20$. The thickness ratios are $R_\alpha/h = 1000, 100, 10$. The cylinder has the same radii of curvature of the cylindrical shell panel, but it is closed in circumferential direction that means $a = 2\pi R_\alpha$. The other dimension is $b = 100$. The thickness ratios are $R_\alpha/h = 1000, 100, 10$. The last geometry is the spherical shell panel with radii of curvature $R_\alpha = R_\beta = 10$, dimensions $a = b = \frac{\pi}{3} R_\alpha$, and thickness ratios $R_\alpha/h = 1000, 100, 10$. All these structures are simply supported. Each geometry includes two different material configurations (see Figure 5). The first material configuration is a one-layered functionally graded material structure where the bottom is fully metallic (m) (Aluminium Alloy Al2024: Young modulus $E_m = 73GPa$, mass density $\rho_m = 2800kg/m^3$ and Poisson ratio $\nu_m = 0.3$) and the top is fully ceramic (c) (Alumina Al_2O_3: Young modulus $E_c = 380GPa$, mass density $\rho_c = 3800kg/m^3$ and Poisson ratio $\nu_c = 0.3$). The Poisson ratio is constant through the thickness. Mass density and Young modulus vary through the thickness by means of the law indicated in Eqs.(79)-(80) where the volume fraction considered is that indicated in Eq.(82) for the ceramic phase ($V_c = 0$ at the bottom and $V_c = 1$ at the top). The exponents p used for the material law are p=0.0, 0.5, 1.0, 2.0. p=0.0 means fully ceramic structure. The second material configuration is a sandwich structure with two external skins with a thickness of $h_1 = h_3 = 0.15h$ and an internal FGM core with a thickness of $h_2 = 0.7h$. The bottom skin is metallic (Aluminum Alloy Al2024) and the top skin is ceramic (Young modulus $E_c = 200GPa$, mass density $\rho_c = 5700kg/m^3$ and Poisson ratio $\nu_c = 0.3$). The functionally graded core has constant Poisson ratio. Mass density and Young modulus have the same variation already indicated for the first material configuration. The p exponents are 0.5, 1.0 and 2.0. A classical core is also considered with material properties $E = \frac{E_c + E_m}{2}$, $\rho = \frac{\rho_c + \rho_m}{2}$ and Poisson ratio $\nu = 0.3$. Figure 6 shows the thickness variation for volume fraction of ceramic phase, Young modulus and mass density for the one-layered FGM structures (first line) and the thickness variation for the sandwich structures embedding an FGM core (second line). Eight different benchmarks are proposed to show a complete overview of the free vibration analysis of one-layered and sandwich FGM plates and shells: one-layered FGM plate (see Table 3 and Figure 7), one-layered FGM cylindrical shell panel (see Table 4 and Figure 8), one-layered FGM cylinder (see Table 5), one-layered FGM spherical shell panel (see Table 6), sandwich FGM plate (see Table 7), sandwich FGM cylindrical shell panel (see Table 8), sandwich FGM cylinder (see Table 9 and Figure 9), sandwich FGM spherical shell panel (see Table 10 and Figure 10). The first three circular frequencies in non-dimensional form ($\bar{\omega} = \omega(\frac{a}{h})^2\sqrt{\frac{\rho_c}{E_c}}$ for plate geometry and $\bar{\omega} = \frac{\omega}{10}(\frac{R_\alpha}{h})^2\sqrt{\frac{\rho_c}{E_c}}$ for shell geometries) are calculated in Tables 3-10 for various pairs of half-wave numbers (m,n), several thickness ratios and various exponents p for the material law. The vibration modes plotted in Figs. 7-10 are given in terms of non-dimensional values such as $u^* = u/|u_{max}|$, $v^* = v/|v_{max}|$, $w^* = w/|w_{max}|$ and $z^* = \tilde{z}/h$.

Table 3 presents thick and thin square one-layered FGM plates (Benchmark 1). The first three vibration modes are shown for half-wave numbers m=n=1,2,3. Different thickness ratios and exponents p of the FGM law are investigated. For each vibration mode and thickness ratio, the biggest frequencies are obtained for the case of full ceramic material (p=0.0). The frequencies decrease in the case of FGM

material from p=0.5 to p=2.0. Each frequency (from the first to the third one) increases with the increase of the half-wave numbers (m,n). Figure 7 shows the first three vibration modes in terms of displacements for the one-layered FGM plate in the cases of half-wave numbers m=n=1,2,3 and exponent for the material law p=1.0. The first mode has linear in-plane displacements (u^*, v^*) and constant transverse displacement (w^*) through the thickness for each pair of half-wave numbers. The second mode has zero transverse displacement (in-plane vibration mode) and constant in-plane displacements through the thickness for each pair of half-wave numbers. The third mode has constant in-plane displacements and linear transverse displacement through the thickness for each pair of half-wave numbers. When the half-wave numbers increase the constant displacements become quasi-constant displacements and the linear displacements become quasi-linear displacements. The frequency values in Table 3 are obtained by dividing the plate into $N_L = 100$ mathematical layers. The same number of mathematical layers are used for results in Table 4 (Benchmark 2), Table 5 (Benchmark 3) and Table 6 (Benchmark 4) for one-layered FGM cylindrical shell panel, cylinder and spherical shell panel, respectively. The behavior of shell structures is similar to that shown for plates. For each vibration mode and thickness ratio, the biggest frequencies are obtained for fully ceramic material (p=0.0). For FGM materials, the frequencies decrease from p=0.5 to p=2.0. Each frequency (from the first to the third one) increases with the increase of the half-wave numbers (m,n). For cylinders, half-wave number m can assume only even values (e.g., m=2 in Table 5) because the structure is closed in α-direction. Half-wave number n in β-direction has values 1, 2 and 3. Figure 8 shows the first three vibration modes in terms of displacements for the one-layered FGM cylindrical shell panel for half-wave numbers m=n=1,2,3 and exponent for material law p=0.5. The first mode has linear or quasi-linear in-plane displacements (u^*, v^*) and constant or quasi-constant transverse displacement (w^*) through the thickness for each pair of half-wave numbers. The second mode has constant or quasi-constant in-plane and transverse displacements through the thickness for each pair of half-wave numbers. The effect of the curvature gives a second vibration mode for the cylindrical shell panel that is not an in-plane mode as in the case of plate shown in Figure 7. The plate has the same radii of curvature because both R_α and R_β are infinite. The cylindrical shell panel has two different radii of curvature, $R_\alpha = 10$ and infinite R_β radius of curvature in longitudinal direction. The third mode has constant or quasi-constant in-plane displacements through the thickness and linear transverse displacement through the thickness. The effect of half-wave numbers is the one already shown for the plate case seen in Figure 7.

Table 7 shows thick and thin square sandwich plates with an FGM core (Benchmark 5). The first three vibration modes are calculated for half-wave numbers m=n=1,2,3 and for different thickness ratios and exponents p of the FGM law (the use of a classical core is also analyzed). A different ceramic material is considered in Benchmarks 5-8 for sandwich cases. The behavior in terms of vibration modes is similar to the one-layered cases. Some small differences are due to the fact that the skins are in classical materials and the FGM layer has a different ceramic phase even if the FGM law is the one already seen for the one-layered case. Minor differences are shown for the first vibration mode (I) that does not decrease when exponent p increases. It is clear how the FGM behavior depends on both the FGM law through the thickness and the materials of the two phases. The behavior seen for the plate case in Table 7 is similar to the behaviors shown in Table 8 (Benchmark 6), Table 9 (Benchmark 7) and Table 10 (Benchmark 8) for sandwich FGM cylindrical shell panel, cylinder and spherical shell panel, respectively. Each vibration mode for a given thickness ratio and pair of half-wave numbers (m,n) always has frequency values that decrease when the p value increases. The classical core, with material properties that are an average between ceramic and metal properties, gives frequencies similar to those obtained with an FGM core with $p = 1.0$ (linear thickness law for elastic properties). The frequency values are obtained by dividing the FGM core into 80 mathematical layers and each classical skin into 10 mathematical layers. Mathematical layers are used to correctly consider both FGM material law and curvature effects. This splitting into mathematical layers is the same for both plate and shell geometries. Figure 9 shows the first three vibration modes for half-wave numbers m=n=2 and sandwich cylinder.

FGM cores with exponent for material law p=1.0 are compared with classical cores. For both cases the first mode has constant through-the-thickness in-plane circumferential displacement and transverse displacement and linear through-the-thickness in-plane longitudinal displacement. The second mode has constant through-the-thickness in-plane longitudinal displacement and transverse displacement and linear through-the-thickness in-plane circumferential displacement (for both types of core). The third mode has quasi-constant in-plane displacements and transverse displacements (for both types of core). The cylinder is closed in α-direction with one of the two radii of curvature that is infinite. R_α different from R_β gives the second vibration mode that is not an in-plane mode. The plate case in Figure 7 (both infinite radii of curvature, that means the same values of R_α and R_β) has an in-plane second vibration mode. Figure 10 shows the first three vibration modes for half-wave numbers m=n=3 for sandwich spherical shell panel. The FGM core with exponent for material law p=2.0 is compared with classical core. There are no differences in terms of vibration modes for the two core configurations. The imposed half-wave numbers considered in this example have higher values. Therefore, the displacements are quasi-linear or quasi-constant. The first vibration mode has quasi-linear in-plane displacements and quasi-constant transverse displacement through the thickness. The second vibration mode is an in-plane mode (zero transverse displacement) as in the plate case of Figure 7 because the structure has coincident ($R_\alpha = R_\beta = 10$) radii of curvature (see the comparison with the cylinder case in Figure 9). In-plane displacements are quasi-constant through the thickness. The third vibration mode has linear transverse displacement through the thickness and quasi-constant in-plane displacements through the thickness.

The use of an FGM layer allows the change of frequency values without any change in the behavior of the structure in terms of vibration modes.

5 Conclusions

The general three-dimensional formulation proposed in this paper uses an exact geometry for shells and a layer-wise approach for the multilayered FGM structures. The differential equations of equilibrium in orthogonal curvilinear coordinates for the free vibrations of simply supported plates and shells have been exactly solved in three-dimensional form. This method allows free vibration results for spherical, open cylindrical, closed cylindrical and flat panels to be obtained. The layer-wise approach proposed is based on the continuity of displacements and transverse shear/normal stresses at the interfaces between the layers of the plates and shells. This approach allows the solution of equilibrium equations for FGM shells by introducing several mathematical layers where material properties and parametric coefficients for the shell geometry description can be assumed as constant. Therefore, they do not depend on the thickness coordinate. One-layered FGM structures and sandwich plates and shells with external classical skins and an internal FGM core have been investigated. The first three vibration modes have been shown for several geometries, material configurations, various thickness ratios and half-wave numbers imposed. The introduction of FGM layers allows the change of frequency values but the behavior of the structure in terms of vibration modes remains the same. These results will be useful benchmarks to validate future refined 2D models for the free vibration analysis of FGM structures. Furthermore, this exact solution gives a global three-dimensional overview of the free vibration problem of FGM plates and shells.

Bibliography

Alibeigloo, A.; Kani, A.M.; Pashaei, M.H. (2012): Elasticity solution for the free vibration analysis of functionally graded cylindrical shell bonded to thin piezoelectric layers. *International Journal of Pressure Vessels and Piping*, vol. 89, pp. 98-111.

Batra, R.C.; Jin, J. (2005): Short Communication. Natural frequencies of a functionally graded anisotropic rectangular plate. *Journal of Sound and Vibration*, vol. 282, pp. 509-516.

Birman, V.; Byrd, L.W. (2007): Modeling and analysis of functionally graded materials and structures. *Applied Mechanics Reviews*, vol. 60, pp. 195-216.
Bishay, P.L.; Atluri, S.N. (2012): High-performance 3D hybrid/mixed, and simple 3D Voronoi cell finite elements, for macro- & micro-mechanical modeling of solids, without using multi-field variational principles. *CMES: Computer Modeling in Engineering & Sciences*, vol. 84, pp. 41-97.
Bishay P.L.; Sladek, J.; Sladek, V.; Atluri, S.N. (2012): Analysis of functionally graded magneto-electro-elastic composites using hybrid/mixed finite elements and node-wise material properties. *CMC: Computers, Materials & Continua*, vol. 29, pp. 213-262.
Boyce, W.E.; DiPrima, R.C. (2001): Elementary Differential Equations and Boundary Value Problems, John Wiley & Sons, Inc., New York, USA.
Brischetto, S. (2009): Classical and mixed advanced models for sandwich plates embedding functionally graded cores. *Journal of Mechanics of Materials and Structures*, vol. 4, pp. 13-33.
Brischetto, S.; Carrera, E. (2010): Advanced mixed theories for bending analysis of functionally graded plates. *Computers and Structures*, vol. 88, pp. 1474-1483.
Brischetto, S.; Leetsch, R.; Carrera, E.; Wallmersperger, T.; Kröplin, B. (2008): Thermo-mechanical bending of functionally graded plates. *Journal of Thermal Stresses*, vol. 31, pp. 286-308.
Cao, Z.-Y.; Wang, H.-N. (2007): Free vibration of FGM cylindrical shells with holes under various boundary conditions. *Journal of Sound and Vibration*, vol. 306, pp. 227-237.
Carrera, E.; Brischetto, S. (2009): A survey with numerical assessment of classical and refined theories for the analysis of sandwich plates. *Applied Mechanics Reviews*, vol. 62, pp. 1-17.
Carrera, E.; Brischetto, S.; Nali, P. (2011): Plates and Shells for Smart Structures. Classical and Advanced Theories for Modeling and Analysis, John Wiley & Sons, Ltd, New Delhi, India.
Carrera, E.; Brischetto, S.; Robaldo, A. (2008): Variable kinematic model for the analysis of functionally graded material plates. *AIAA Journal*, vol. 46, pp. 194-203.
Chen, W.Q.; Bian, Z.G.; Ding, H.J. (2004): Three-dimensional vibration analysis of fluid-filled orthotropic FGM cylindrical shells. *International Journal of Mechanical Sciences*, vol. 46, pp. 159-171.
Dong, C.Y. (2008): Three-dimensional free vibration analysis of functionally graded annular plates using the Chebyshev-Ritz method. *Materials and Design*, vol. 29, pp. 1518-1525.
Dong, L.; Atluri, S.N. (2011): A simple procedure to develop efficient & stable hybrid/mixed elements, and Voronoi cell finite elements for macro- & micro-mechanics. *CMC: Computers Materials & Continua*, vol. 24, pp. 61-104.
Dozio, L. (2013): Natural frequencies of sandwich plates with FGM core via variable-kinematic 2-D Ritz models. *Composite Structures*, vol. 96, pp. 561-568.
Efraim, E.; Eisenberger, M. (2007): Exact vibration analysis of variable thickness thick annular isotropic and FGM plates. *Journal of Sound and Vibration*, vol. 299, pp. 720-738.
Hildebrand, F.B.; Reissner, E.; Thomas, G.B. (1949): Notes on the Foundations of the Theory of Small Displacements of Orthotropic Shells, NACA Technical Note No. 1833, Washington D.C., USA.
Hosseini-Hashemi, S.; Salehipour, H.; Atashipour, S.R. (2012): Exact three-dimensional free vibration analysis of thick homogeneous plates coated by a functionally graded layer. *Acta Mechanica*, vol. 223, pp. 2153-2166.
Hosseini-Hashemi, S.; Fadaee, M.; Atashipour, S.R. (2011): Study on the free vibration of thick functionally graded rectangular plates according to a new exact closed-form procedure. *Composite Structures*, vol. 93, pp. 722-735.
Kashtalyan, M. (2004): Three-dimensional elasticity solution for bending of functionally graded rectangular plates. *European Journal of Mechanics A/Solids*, vol. 23, pp. 853-864.
Kashtalyan, M.; Menshykova, M. (2009): Three-dimensional elasticity solution for sandwich panels with a functionally graded core. *Composite Structures*, vol. 87, pp. 36-43.
Leissa, A.W. (1969): Vibration of Plates, NASA SP-160, Washington D.C., USA.
Leissa, A.W. (1973): Vibration of Shells, NASA SP-288, Washington D.C., USA.

Li, Q.; Iu, V.P.; Kou, K.P. (2008): Three-dimensional vibration analysis of functionally graded material sandwich plates. *Journal of Sound and Vibration*, vol. 311, pp. 498-515.
Loy, C.T.; Lam, K.Y.; Reddy, J.N. (1999): Vibration of functionally graded cylindrical shells. *International Journal of Mechanical Sciences*, vol. 41, pp. 309-324.
Malekzadeh, P. (2009): Three-dimensional free vibration analysis of thick functionally graded plates on elastic foundations. *Composite Structures*, vol. 89, pp. 367-373.
Matsunaga, H. (2008): Free vibration and stability of functionally graded plates according to a 2-D higher-order deformation theory. *Composite Structures*, vol. 82, pp. 499-512.
Matsunaga, H. (2009): Free vibration and stability of functionally graded circular cylindrical shells according to a 2D higher-order deformation theory. *Composite Structures*, vol. 88, pp. 519-531.
Mattei, G.; Tirella, A.; Ahluwalia, A. (2012): Functionally Graded Materials (FGMs) with predictable and controlled gradient profiles: computational modelling and realisation. *CMES: Computer Modeling in Engineering & Sciences*, vol. 87, pp. 483-504.
Messina, A. (2009): Three Dimensional Free Vibration Analysis of Cross-Ply Laminated Plates through 2D and Exact Models. *3rd International Conference on Integrity, Reliability and Failure*, Porto (Portugal).
Moler, C.; Van Loan, C. (2003): Nineteen dubious ways to compute the exponential of a matrix, twenty-five years later. *SIAM Review*, vol. 45, pp. 1-46.
Nie, G.J.; Zhong, Z. (2008): Vibration analysis of functionally graded annular sectorial plates with simply supported radial edges. *Composite Structures*, vol. 84, pp. 167-176.
Open document, free available on http://www.math.utah.edu/gustafso/, accessed on 10th October 2013. Systems of Differential Equations.
Pradyumna, S.; Bandyopadhyay, J.N. (2008): Free vibration analysis of functionally graded curved panels using a higher-order finite element formulation. *Journal of Sound and Vibration*, vol. 318, pp. 176-192.
Shariyat, M. (2009): Vibration and dynamic buckling control of imperfect hybrid FGM plates with temperature-dependent material properties subjected to thermo-electro-mechanical loading conditions. *Composite Structures*, vol. 88, pp. 240-252.
Sladek, J.; Sladek, V.; Krivacek, J.; Zhang, C. (2005): Meshless local Petrov-Galerkin method for stress and crack analysis in 3-D axisymmetric FGM bodies. *CMES: Computer Modeling in Engineering & Sciences*, vol. 8, pp. 259-270.
Sladek, J.; Sladek, V.; Tan, C.L.; Atluri, S.N. (2008): Analysis of transient heat conduction in 3D anisotropic functionally graded solids, by the MLPG method. *CMES: Computer Modeling in Engineering & Sciences*, vol. 32, pp. 161-174.
Sladek, J.; Sladek, V.; Solek, P. (2009): Elastic analysis in 3D anisotropic functionally graded solids by the MLPG. *CMES: Computer Modeling in Engineering & Sciences*, vol. 43, pp. 223-252.
Soedel, W. (2005): Vibration of Shells and Plates, Marcel Dekker, Inc., New York, USA.
Soldatos, K.P.; Ye, J. (1995): Axisymmetric static and dynamic analysis of laminated hollow cylinders composed of monoclinic elastic layers. *Journal of Sound and Vibration*, vol. 184, pp. 245-259.
Tornabene, F. (2012): Meccanica delle Strutture a Guscio in Materiale Composito, Societá Editrice Esculapio, Bologna, Italy.
Vel, S.S. (2010): Exact elasticity solution for the vibration of functionally graded anisotropic cylindrical shells. *Composite Structures*, vol. 92, pp. 2712-2727.
Vel, S.S.; Batra, R.C. (2004): Three-dimensional exact solution for the vibration of functionally graded rectangular plates. *Journal of Sound and Vibration*, vol. 272, pp. 703-730.
Wu, C.-P.; Chiu, K.-H. (2011): RMVT-based meshless collocation and element-free Galerkin methods for the quasi-3D free vibration analysis of multilayered composite and FGM plates. *Composite Structures*, vol. 93, pp. 1433-1448.
Wu, C.-P.; Jiang, R.-Y. (2012): A state space differential reproducing kernel method for the 3D

analysis of FGM sandwich circular hollow cylinders with combinations of simply-supported and clamped edges. *Composite Structures*, vol. 94, pp. 3401-3420.
Xia, X.-K.; Shen, H.-S. (2008): Vibration of post-buckled sandwich plates with FGM face sheets in a thermal environment. *Journal of Sound and Vibration*, vol. 314, pp. 254-274.
Xu, Y.; Zhou, D. (2009): Three-dimensional elasticity solution of functionally graded rectangular plates with variable thickness. *Composite Structures*, vol. 91, pp. 56-65.
Zahedinejad, P.; Malekzadeh, P.; Farid, M.; Karami, G. (2010): A semi-analytical three-dimensional free vibration analysis of functionally graded curved panels. *International Journal of Pressure Vessels and Piping*, vol. 87, pp. 470-480.
Zenkour, A.M. (2005a): A comprehensive analysis of functionally graded sandwich plates: Part 1-Deflection and stresses. *International Journal of Solids and Structures*, vol. 42, pp. 5224-5242.
Zenkour, A.M. (2005b): A comprehensive analysis of functionally graded sandwich plates: Part 2-Buckling and free vibration. *International Journal of Solids and Structures*, vol. 42, pp. 5243-5258.
Zhao, X.; Lee, Y.Y.; Liew, K.M. (2009): Free vibration analysis of functionally graded plates using the element-free *kp*-Ritz method. *Journal of Sound and Vibration*, vol. 319, pp. 918-939.
Zhong, Z.; Shang, E.T. (2003): Three-dimensional exact analysis of a simply supported functionally gradient piezoelectric plate. *International Journal of Solids and Structures*, vol. 40, pp. 5335-5352.
Zwillinger, D. (1997): Handbook of Differential Equations, Academic Press, New York, USA.

p	0.5	1.0	2.0	5.0	10
			$a/h = 100$		
Li et al. (2008)	1.33931	1.38669	1.44491	1.53143	1.59105
Present 3D	1.33928	1.38671	1.44494	1.53148	1.59113
			$a/h = 10$		
Li et al. (2008)	1.29751	1.34847	1.40828	1.49309	1.54980
Present 3D	1.29748	1.34848	1.40829	1.49311	1.54984
			$a/h = 5$		
Li et al. (2008)	1.19580	1.25338	1.31569	1.39567	1.44540
Present 3D	1.19575	1.25337	1.31566	1.39564	1.44537

Table 1: First assessment: sandwich plate with FGM core. Fundamental circular frequency $\bar{\omega} = \omega \frac{a^2}{h}\sqrt{\frac{\rho_0}{E_0}}$ for half-wave numbers m=n=1 and different thickness ratios a/h and exponents p for the material law. Comparison between 3D model based on Ritz approach by Li et al. (2008) and the present 3D exact solution.

p	0.0	0.5	1.0	4.0	10
			$a/R_\alpha = 0.5$		
Zahedinejad et al. (2010)	0.2113	0.1814	0.1639	0.1367	0.1271
Present 3D	0.2129	0.1817	0.1638	0.1374	0.1296
			$a/R_\alpha = 1.0$		
Zahedinejad et al. (2010)	0.2164	0.1852	0.1676	0.1394	0.1286
Present 3D	0.2155	0.1848	0.1671	0.1392	0.1300

Table 2: Second assessment: one-layered FGM cylindrical shell panel with thickness ratio a/h=5. Fundamental circular frequency $\bar{\omega} = \omega h\sqrt{\frac{\rho_c}{E_c}}$ for half-wave numbers m=n=1 and different radii of curvature R_α and exponents p for the material law. Comparison between 3D model based on the differential quadrature method by Zahedinejad et al. (2010) and the present 3D exact solution.

p		0.0			0.5			1.0			2.0	
a/h	100	20	5	100	20	5	100	20	5	100	20	5
						m=n=1						
I	5.9713	5.9219	5.3036	5.0502	5.0126	4.5316	4.5529	4.5193	4.0923	4.1453	4.1118	3.6943
II	275.53	55.107	13.777	246.60	49.316	12.312	228.27	45.643	11.368	206.11	41.202	10.225
III	465.73	93.113	23.136	416.82	83.325	20.666	385.84	77.106	19.026	348.37	69.578	17.010
						m=n=2						
I	23.860	23.108	16.882	20.182	19.603	14.644	18.195	17.681	13.278	16.564	16.054	11.876
II	551.07	110.21	27.554	493.20	98.605	24.514	456.53	91.219	22.453	412.19	82.284	19.955
III	931.42	186.01	45.071	833.60	166.39	40.106	771.60	153.82	36.330	696.63	138.55	31.591
						m=n=3						
I	53.592	50.055	30.318	45.338	42.605	26.597	40.874	38.447	24.217	37.206	34.813	21.574
II	826.61	165.32	41.330	739.78	147.84	36.483	684.76	136.66	32.945	618.23	123.12	28.763
III	1397.0	278.46	62.671	1250.3	248.94	56.109	1157.2	229.73	50.081	1044.6	206.29	42.333

Table 3: Benchmark 1. One-layered FGM plate, first three circular frequencies $\bar{\omega} = \omega(\frac{a}{h})^2\sqrt{\frac{\rho_c}{E_c}}$ for different half-wave numbers (m,n), thickness ratios a/h and exponents p for the material law.

p		0.0			0.5			1.0			2.0	
R_α/h	1000	100	10	1000	100	10	1000	100	10	1000	100	10
						m=n=1						
I	2031.0	20.520	0.3534	1817.8	18.350	0.3038	1682.7	16.981	0.2760	1519.3	15.336	0.2500
II	21561	215.61	2.1571	19297	192.92	1.9255	17862	178.57	1.7799	16128	161.22	1.6053
III	36634	366.33	3.6530	32788	327.97	3.2799	30352	303.67	3.0415	27406	274.26	2.7501
						m=n=2						
I	2123.8	25.032	1.2578	1900.4	22.060	1.0633	1759.0	20.282	0.9562	1588.3	18.351	0.8632
II	42304	423.04	4.2325	37861	378.54	3.7780	35047	350.37	3.4900	31644	316.33	3.1437
III	71558	715.54	7.1145	64046	640.63	6.3900	59288	593.16	5.9166	53533	535.70	5.3319
						m=n=3						
I	2159.1	37.340	2.6535	1930.3	32.178	2.2545	1786.1	29.278	2.0288	1612.9	26.568	1.8233
II	63208	632.08	6.3235	56569	565.58	5.6418	52364	523.49	5.2039	47280	472.63	4.6765
III	106869	1068.6	10.570	95650	956.71	9.4929	88543	885.79	8.7632	79950	799.93	7.8492

Table 4: Benchmark 2. One-layered FGM cylindrical shell panel, first three circular frequencies $\bar{\omega} = \frac{\omega}{10}(\frac{R_\alpha}{h})^2\sqrt{\frac{\rho_c}{E_c}}$ for different half-wave numbers (m,n), thickness ratios R_α/h and exponents p for the material law.

p		0.0			0.5			1.0			2.0	
R_α/h	1000	100	10	1000	100	10	1000	100	10	1000	100	10
						m=2, n=1						
I	619.55	6.1956	0.0620	554.55	5.5499	0.0560	513.35	5.1399	0.0521	463.54	4.6429	0.0472
II	6907.6	69.077	0.6910	6182.0	61.801	0.6162	5722.5	57.197	0.5694	5166.8	51.638	0.5134
III	14993	149.93	1.4972	13418	134.17	1.3384	12421	124.19	1.2385	11215	112.14	1.1184
						m=2, n=2						
I	1953.5	19.535	0.1957	1748.5	17.496	0.1763	1618.6	16.202	0.1638	1461.5	14.634	0.1484
II	8453.9	84.539	0.8457	7566.0	75.643	0.7549	7003.5	70.012	0.6979	6323.6	63.209	0.6296
III	15541	155.41	1.5521	13909	139.08	1.3887	12875	128.75	1.2857	11625	116.26	1.1615
						m=2, n=3						
I	3428.8	34.289	0.3437	3068.9	30.704	0.3090	2840.9	28.430	0.2869	2565.2	25.678	0.2597
II	10153	101.53	1.0155	9086.3	90.845	0.9069	8410.9	84.085	0.8386	7594.3	75.916	0.7566
III	16589	165.88	1.6570	14847	148.48	1.4845	13743	137.46	1.3754	12409	124.13	1.2432

Table 5: Benchmark 3. One-layered FGM cylinder, first three circular frequencies $\bar{\omega} = \frac{\omega}{10}(\frac{R_\alpha}{h})^2\sqrt{\frac{\rho_c}{E_c}}$ for different half-wave numbers (m,n), thickness ratios R_α/h and exponents p for the material law.

p		0.0			0.5			1.0			2.0	
R_α/h	1000	100	10	1000	100	10	1000	100	10	1000	100	10
						m=n=1						
I	9541.6	95.526	1.0545	8538.8	85.403	0.9257	7903.8	79.010	0.8488	7136.1	71.308	0.7637
II	26312	263.11	2.6256	23550	235.56	2.3578	21800	218.11	2.1875	19684	197.00	1.9796
III	46612	466.10	4.6344	41720	417.42	4.1745	38621	386.56	3.8775	34873	349.19	3.5105
						m=n=2						
I	9885.5	101.01	2.1222	8846.2	90.103	1.8093	8188.2	83.274	1.6329	7392.9	75.174	1.4678
II	52623	526.22	5.2508	47099	471.12	4.7134	43600	436.22	4.3673	39368	393.97	3.9438
III	90001	899.92	8.9041	80555	805.99	8.0290	74572	746.42	7.4431	67336	674.25	6.7063
						m=n=3						
I	9959.6	110.45	4.0189	8911.7	97.740	3.4273	8248.4	90.016	3.0864	7447.4	81.342	2.7617
II	78935	789.34	7.8750	70649	706.68	7.0644	65399	654.30	6.5313	59052	590.91	5.8765
III	134123	1341.0	13.150	120047	1201.0	11.866	111130	1112.2	10.953	100347	1004.6	9.7779

Table 6: Benchmark 4. One-layered FGM spherical shell panel, first three circular frequencies $\bar{\omega} = \frac{\omega}{10}(\frac{R_\alpha}{h})^2\sqrt{\frac{\rho_c}{E_c}}$ for different half-wave numbers (m,n), thickness ratios R_α/h and exponents p for the material law.

p core		classical			0.5			1.0			2.0	
a/h	100	20	5	100	20	5	100	20	5	100	20	5
						m=n=1						
I	5.5911	5.5460	4.9779	5.3707	5.3327	4.8434	5.3788	5.3384	4.8233	5.4598	5.4137	4.8396
II	263.62	52.723	13.179	267.13	53.425	13.354	263.62	52.722	13.176	259.44	51.886	12.965
III	445.59	89.086	22.139	451.52	90.276	22.450	445.59	89.086	22.143	438.52	87.670	21.771
						m=n=2						
I	22.342	21.653	15.894	21.464	20.880	15.750	21.495	20.876	15.565	21.816	21.114	15.379
II	527.23	105.44	26.350	534.25	106.85	26.691	527.23	105.44	26.323	518.87	103.76	25.887
III	891.13	177.97	43.175	903.01	180.37	43.948	891.13	177.98	43.262	877.00	175.12	42.300
						m=n=3						
I	50.183	46.940	28.602	48.221	45.453	28.713	48.287	45.360	28.241	48.998	45.707	27.640
II	790.85	158.16	39.501	801.38	160.26	39.993	790.84	158.14	39.412	778.31	155.62	38.721
III	1336.6	266.44	60.223	1354.4	270.09	62.220	1336.6	266.46	60.684	1315.4	262.10	57.815

Table 7: Benchmark 5. Sandwich plate embedding an FGM core, first three circular frequencies $\bar{\omega} = \omega(\frac{a}{h})^2\sqrt{\frac{\rho_c}{E_c}}$ for different half-wave numbers (m,n), thickness ratios a/h and exponents p for the material law.

p core		classical			0.5			1.0			2.0	
R_α/h	1000	100	10	1000	100	10	1000	100	10	1000	100	10
						m=n=1						
I	1943.2	19.630	0.3322	1969.1	19.874	0.3255	1943.2	19.619	0.3240	1912.4	19.320	0.3248
II	20628	206.21	2.0564	20902	208.93	2.0807	20627	206.17	2.0516	20300	202.89	2.0179
III	35049	350.41	3.4881	35515	355.04	3.5317	35048	350.36	3.4838	34493	344.81	3.4280
						m=n=2						
I	2031.8	23.806	1.1723	2058.5	23.787	1.1352	2031.5	23.563	1.1313	1999.6	23.381	1.1383
II	40473	404.60	4.0351	41011	409.93	4.0828	40472	404.51	4.0256	39830	398.07	3.9596
III	68461	684.46	6.7966	69373	693.51	6.8845	68460	684.38	6.7906	67376	673.53	6.6801
						m=n=3						
I	2064.9	35.200	2.4760	2090.4	34.452	2.4123	2063.5	34.319	2.3966	2031.9	34.458	2.3969
II	60471	604.52	6.0290	61276	612.49	6.1002	60470	604.38	6.0144	59511	594.77	5.9155
III	102244	1022.2	10.102	103605	1035.7	10.240	102243	1022.0	10.098	100622	1005.8	9.9274

Table 8: Benchmark 6. Sandwich cylindrical shell panel embedding an FGM core, first three circular frequencies $\bar{\omega} = \frac{\omega}{10}(\frac{R_\alpha}{h})^2\sqrt{\frac{\rho_c}{E_c}}$ for different half-wave numbers (m,n), thickness ratios R_α/h and exponents p for the material law.

p core		classical			0.5			1.0			2.0	
R_α/h	1000	100	10	1000	100	10	1000	100	10	1000	100	10
						m=2, n=1						
I	592.79	5.9309	0.0597	600.70	6.0111	0.0606	592.81	5.9330	0.0599	583.42	5.8397	0.0590
II	6608.5	66.061	0.6584	6696.5	66.930	0.6661	6608.4	66.043	0.6567	6503.6	64.992	0.6458
III	14344	143.38	1.4267	14534	145.27	1.4435	14343	143.34	1.4231	14116	141.06	1.3997
						m=2, n=2						
I	1869.1	18.697	0.1879	1894.0	18.949	0.1906	1869.1	18.702	0.1883	1839.5	18.407	0.1855
II	8088.0	80.858	0.8066	8195.6	81.926	0.8164	8087.8	80.842	0.8051	7959.6	79.557	0.7919
III	14868	148.63	1.4798	15066	150.59	1.4975	14868	148.60	1.4766	14632	146.24	1.4525
						m=2, n=3						
I	3280.6	32.814	0.3296	3324.3	33.254	0.3342	3280.6	32.819	0.3301	3228.7	32.301	0.3251
II	9713.1	97.109	0.9690	9842.4	98.393	0.9810	9713.0	97.093	0.9674	9559.0	95.550	0.9517
III	15871	158.67	1.5813	16082	160.76	1.6007	15870	158.64	1.5788	15619	156.12	1.5534

Table 9: Benchmark 7. Sandwich cylinder embedding an FGM core, first three circular frequencies $\bar{\omega} = \frac{\omega}{10}(\frac{R_\alpha}{h})^2\sqrt{\frac{\rho_c}{E_c}}$ for different half-wave numbers (m,n), thickness ratios R_α/h and exponents p for the material law.

p core		classical			0.5			1.0			2.0	
R_α/h	1000	100	10	1000	100	10	1000	100	10	1000	100	10
						m=n=1						
I	9128.2	91.329	0.9980	9249.6	92.514	1.0005	9127.8	91.284	0.9876	8983.1	89.830	0.9752
II	25173	251.66	2.5053	25508	254.98	2.5357	25172	251.62	2.5011	24773	247.63	2.4610
III	44595	445.85	4.4267	45188	451.74	4.4829	44594	445.79	4.4226	43888	438.74	4.3522
						m=n=2						
I	9457.1	96.489	1.9823	9582.6	97.548	1.9399	9456.5	96.299	1.9246	9306.6	94.873	1.9213
II	50346	503.32	5.0106	51016	509.96	5.0713	50345	503.23	5.0019	49547	495.25	4.9216
III	86106	860.85	8.5117	87252	872.23	8.6256	86105	860.75	8.5089	84740	847.13	8.3702
						m=n=3						
I	9527.6	105.17	3.7497	9653.2	105.56	3.6755	9526.4	104.41	3.6384	9375.9	103.29	3.6181
II	75518	754.98	7.5159	76523	764.93	7.6067	75517	754.84	7.5024	74320	742.87	7.3814
III	128318	1282.8	12.583	130027	1299.8	12.768	128317	1282.7	12.590	126284	1262.3	12.372

Table 10: Benchmark 8. Sandwich spherical shell panel embedding an FGM core, first three circular frequencies $\bar{\omega} = \frac{\omega}{10}(\frac{R_\alpha}{h})^2\sqrt{\frac{\rho_c}{E_c}}$ for different half-wave numbers (m,n), thickness ratios R_α/h and exponents p for the material law.

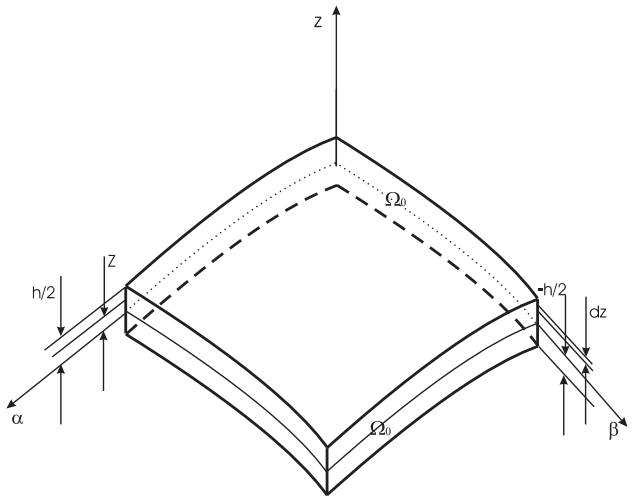

Figure 1: Geometry, notation and reference system for shells.

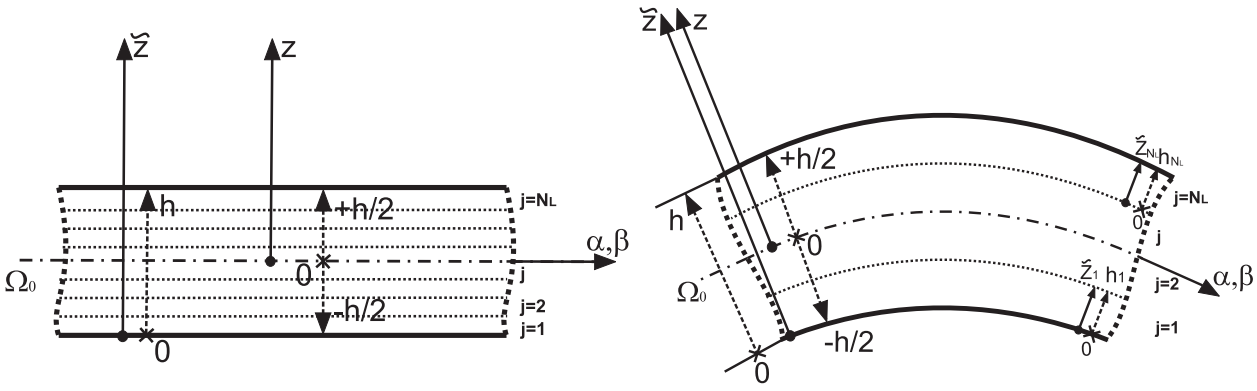

Figure 2: Thickness coordinates and reference systems for mathematical layers in functionally graded plates and shells.

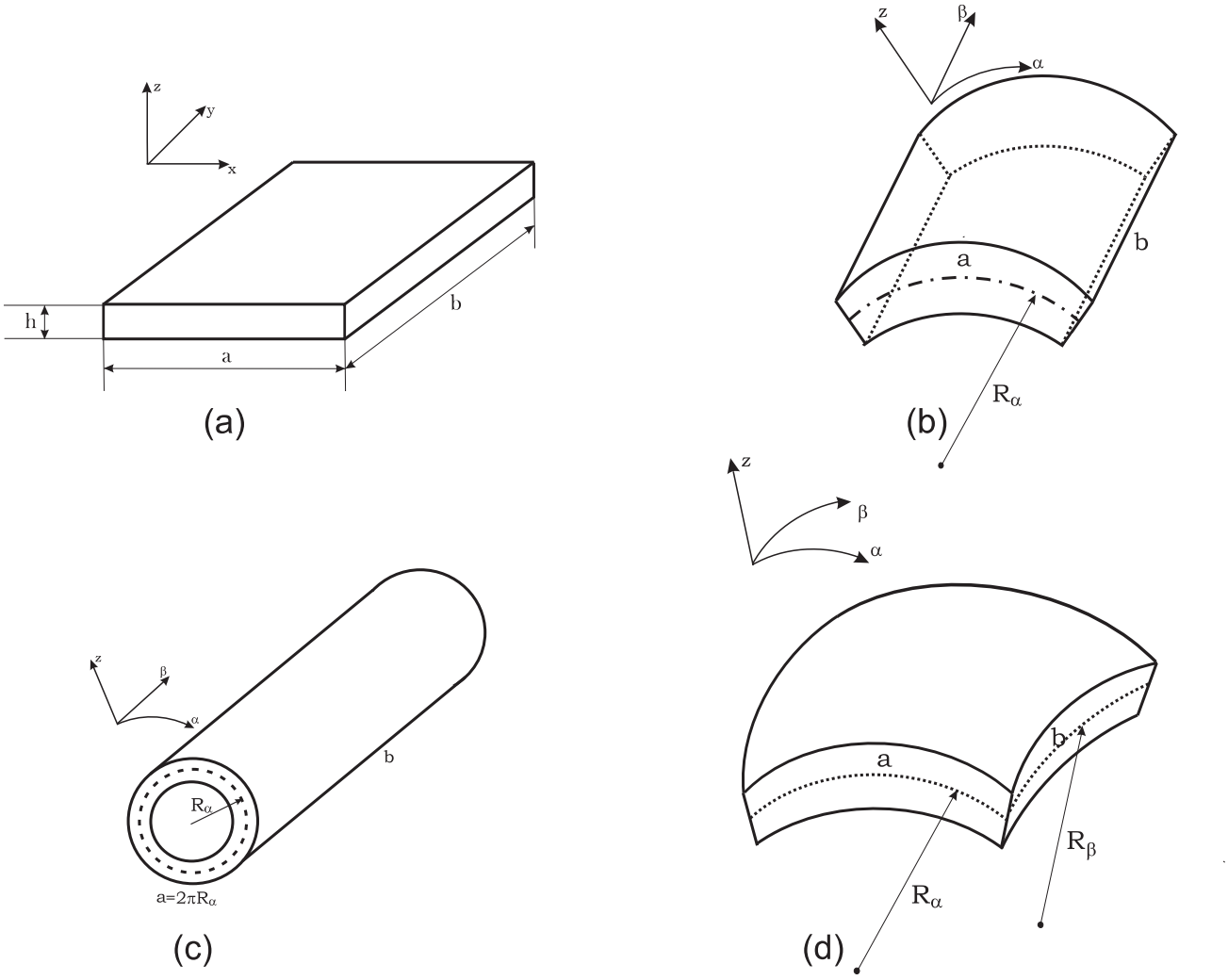

Figure 3: Geometries considered for the assessments and benchmarks: (a) square plate, (b) cylindrical shell panel, (c) cylinder, (d) spherical shell panel.

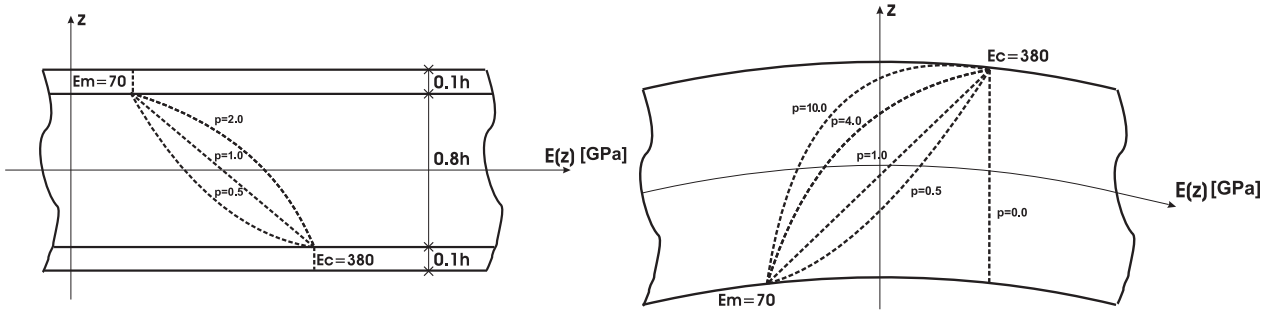

Figure 4: Functionally graded material law through the thickness direction of the sandwich plate for assessment 1 (on the left) and the one-layered cylindrical shell panel for assessment 2 (on the right).

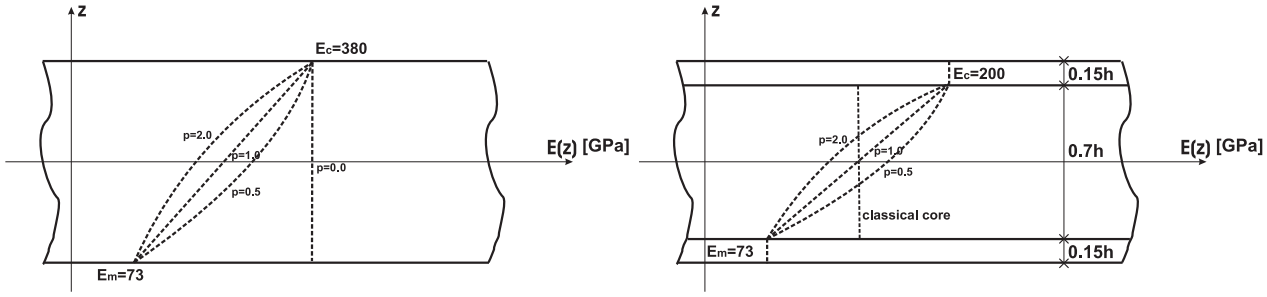

Figure 5: Functionally graded material law through the thickness direction for the one-layered benchmarks (on the left) and sandwich benchmarks (on the right).

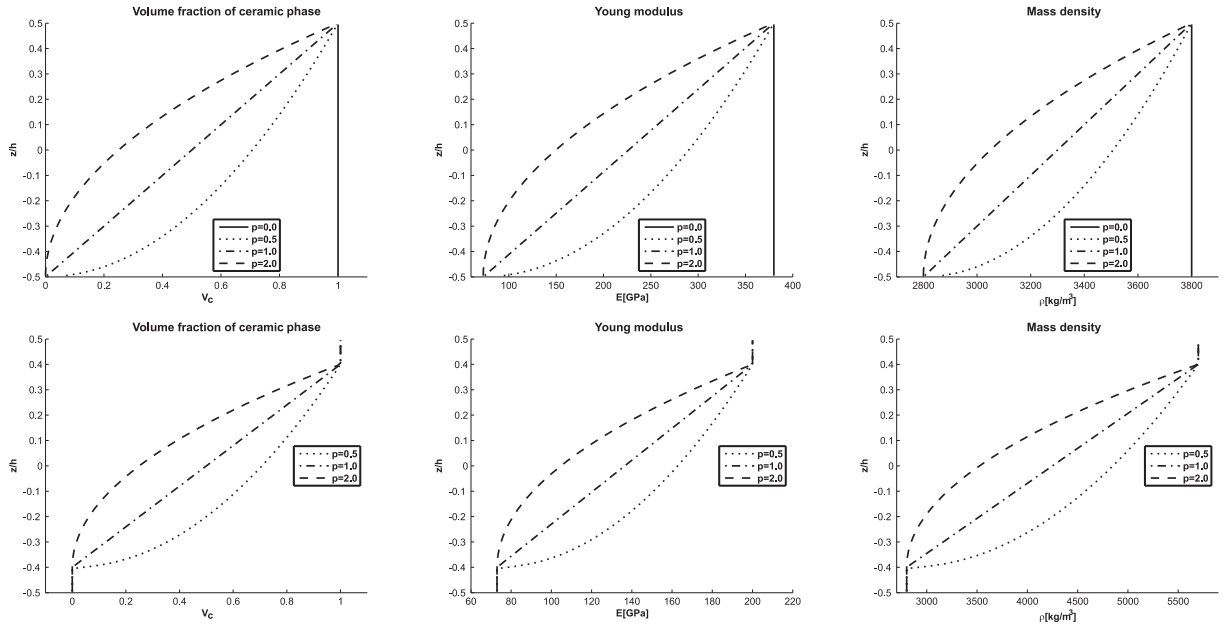

Figure 6: Volume fraction of ceramic phase, Young modulus and mass density through the thickness of the one-layered FGM structures (first row) and through the thickness of the sandwich FGM structures (second row).

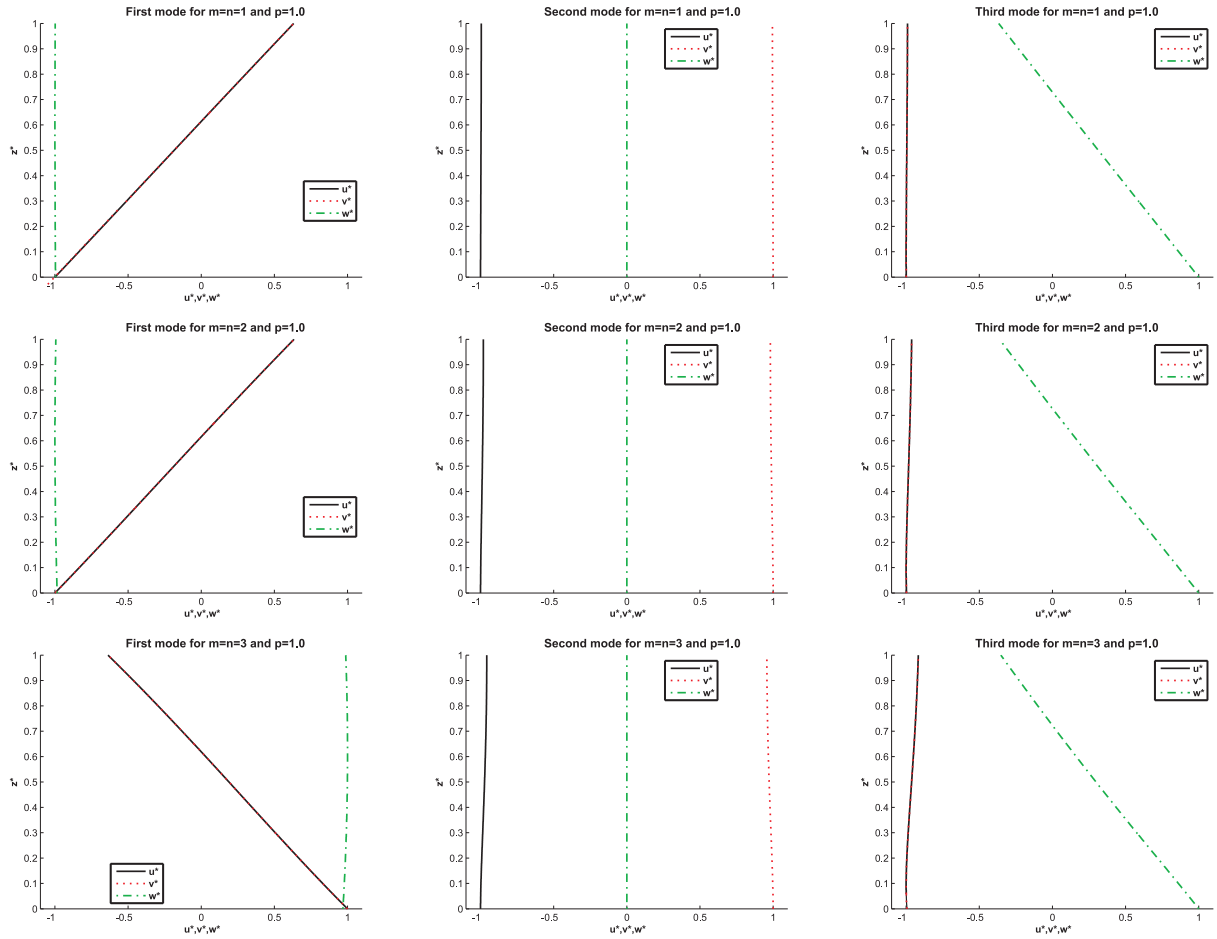

Figure 7: Benchmark 1. One-layered FGM plate, first three modes for thickness ratio a/h=20, exponent for material law p=1.0 and several half-wave numbers (m,n).

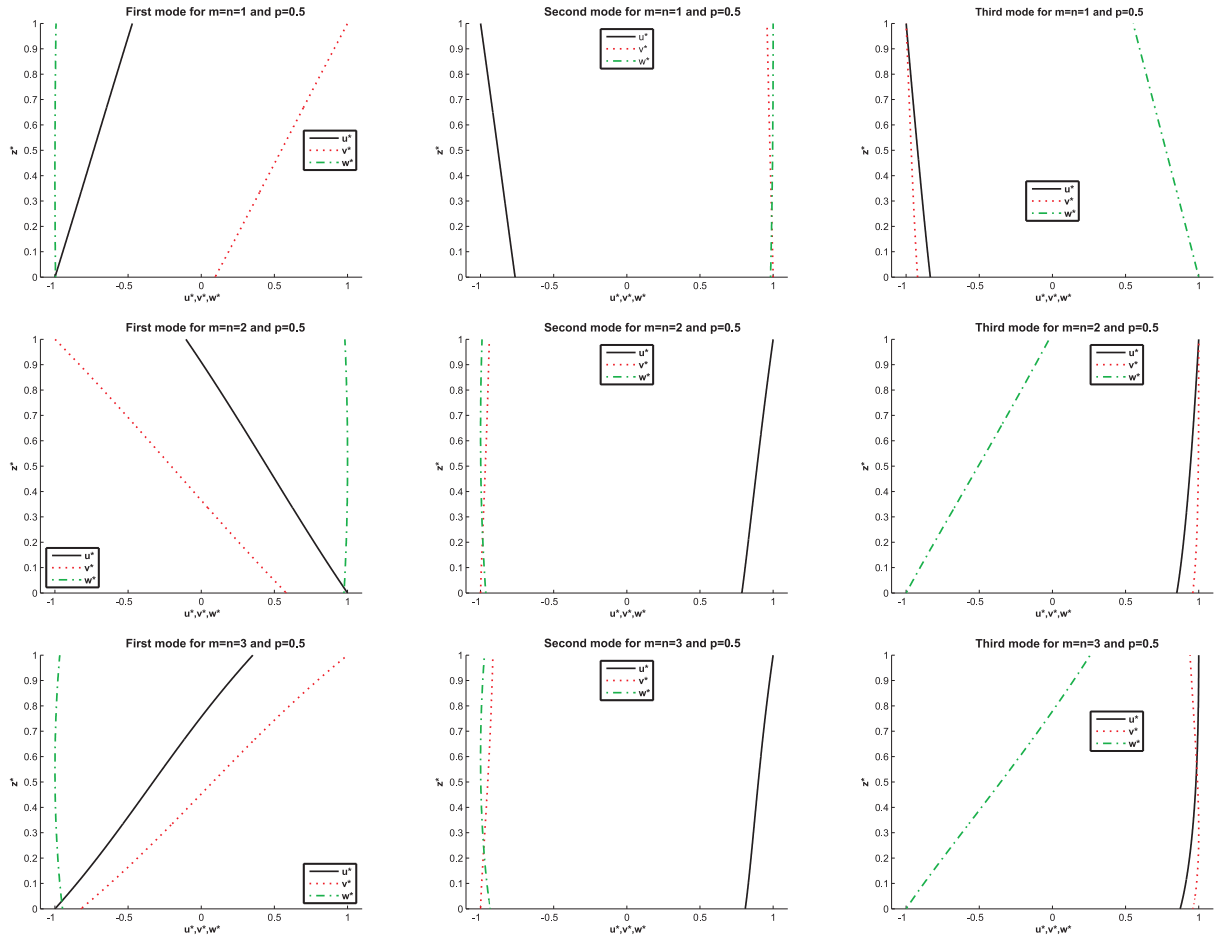

Figure 8: Benchmark 2. One-layered FGM cylindrical shell panel, first three modes for thickness ratio $R_\alpha/h = 10$, exponent for material law p=0.5 and several half-wave numbers (m,n).

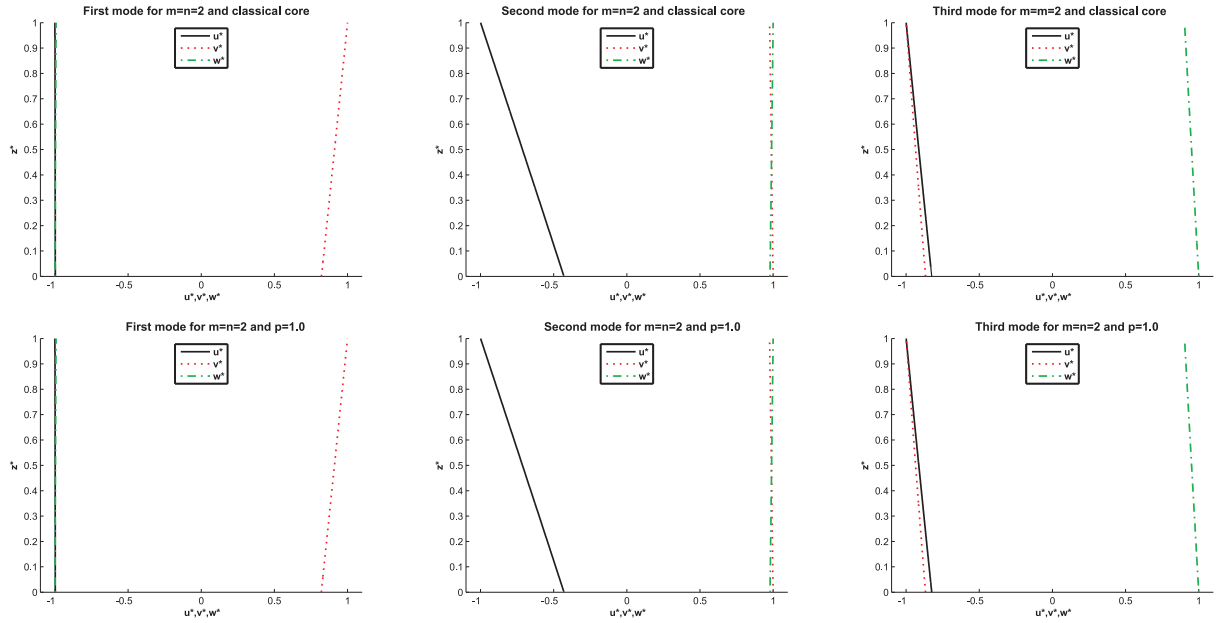

Figure 9: Benchmark 7. Sandwich cylinder, first three modes for thickness ratio $R_\alpha/h = 10$ and half-wave numbers m=n=2. Classical core versus FGM core with exponent for material law p=1.0.

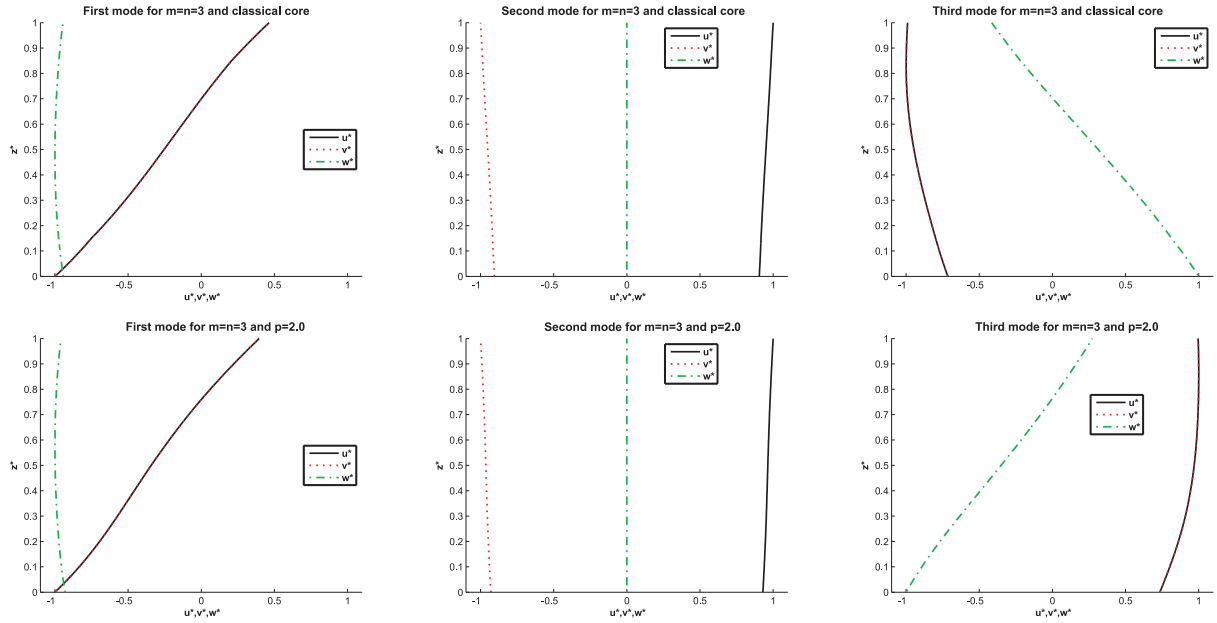

Figure 10: Benchmark 8. Sandwich spherical shell panel, first three modes for thickness ratio $R_\alpha/h = 10$ and half-wave numbers m=n=3. Classical core versus FGM core with exponent for material law p=2.0.